Thermal and wind structure of the Martian thermosphere as given by two General Circulation Models

Francisco González-Galindo, Stephen W. Bougher, Miguel Lopez-Valverde, François Forget, James Murphy

Thermal and wind structure of the Martian thermosphere as given by two General Circulation Models

F. González-Galindo [a,c,*], S.W. Bougher [b], M.A. López-Valverde [a], F. Forget [c], J. Murphy [d]

[a]Instituto de Astrofisica de Andalucia, CSIC, Glorieta de la Astronomia, Granada, Spain
[b]Department of Atmospheric, Oceanic and Planetary Physics, Michigan University, 2455 Hayward Street, Ann Arbor, MI, USA
[c]Laboratoire de Météorologie Dynamique, IPSL, Université Paris 6, BP 99, 4 place Jussieu, Paris, France
[d]Department of Astronomy, New Mexico State University, P.O. Box 30001, MSC 4500, Las Cruces, NM, USA

We have used two different General Circulation Models to study the thermal and wind structure of the Martian upper atmosphere (mesosphere and thermosphere). Both models take into account the effects of waves propagating from the lower atmosphere, although they use different methods for this purpose.

We present the results of three simulations that allow us to take into account the seasonal variability of the Martian atmosphere. Simplified dust scenarios and a common set of input parameters are used.

The temperatures and winds predicted by both models show an overall good agreement. However, some differences have been identified, generally of a local nature. The magnitude of these differences tends to increase with the amount of dust in the lower atmosphere. The different heating terms of the upper atmosphere predicted by both models are in good agreement, which suggests that the differences between the models have their origin in the propagation of waves from the lower atmosphere.

This study has allowed us to confirm the important role of the redistribution of the energy by the winds in producing the longitude–latitude structure of the temperatures. Both models predict also a thermospheric polar warming during the Southern summer solstice, although its intensity seems to be model-dependent and connected to lower atmosphere dust loading.

1. Introduction

During the last decades of the 20th century, the Martian thermosphere remained almost unexplored. We can mention remote sounding of the Martian airglow by Mariner 9 and, as regards in situ data, some individual temperature profiles taken during the entries of Viking Landers (Nier and McElroy, 1977; Seiff and Kirk, 1977), Pathfinder (Schofield et al., 1997; Magalhães et al., 1999) and the Mars Exploration Rovers (Withers and Smith, 2006). However, in the last 10 years, a new suite of data has been taken that have unveiled some interesting aspects of the Martian upper atmosphere although still do not offer a global view of the latitudinal, seasonal, and solar cycle variations.

During the Mars Global Surveyor aerobraking, a tidal structure mainly composed of waves 2 and 3 was observed, and attributed to non-migrating components associated with topography (e.g. Keating et al., 1998; Bougher et al., 2001, 2004; Wilson, 2002; Angelats i Coll et al., 2004). Similar conclusions have been obtained from the analysis of electron profiles measurements by MGS (Bougher et al., 2004). During Mars Odyssey aerobraking, a polar thermospheric warming was observed during Northern winter (Keating et al., 2003), resulting from adiabatic heating from the subsiding branch of a strong interhemispheric circulation cell during solstices (Bougher et al., 2006). The SPICAM instrument on board Mars Express has observed for the first time the NO nightglow on Mars. This emission is produced by the recombination of the N and O atoms, produced in the diurnal upper atmosphere by photodissociation, and transported to the night side (Bertaux et al., 2005), making it a good tracer of the thermospheric dynamics. This instrument has also permitted the study of the upper atmosphere dayglow (Leblanc et al., 2006) and the vertical temperature and density profiles of the mesosphere and the lower thermosphere (Forget et al., 2009; McDunn et al., 2010). The Mars Climate Sounder (MCS) instrument on board Mars Reconnaissance Orbiter (MRO) has observed the propagation of the thermal diurnal tide in the middle atmosphere of Mars (Lee et al., 2009). All these results show signatures of a strong coupling between the upper and lower atmospheres.

Several General Circulation Models for the study of the Martian atmosphere have been developed in the last 40 years, such as the

* Corresponding author at: Instituto de Astrofísica de Andalucía, CSIC, Glorieta de la Astronomía, 18008, Granada, Spain. Tel.: +34 958230527; fax: +34 958814530.
E-mail addresses: ggalindo@iaa.es (F. González-Galindo), bougher@umich.edu (S.W. Bougher), valverde@iaa.es (M.A. López-Valverde), forget@lmd.jussieu.fr (F. Forget), murphy@nmsu.edu (J. Murphy).

NASA Ames MGCM (Pollack et al., 1990; Haberle et al., 1993, 1999), the thermospheric MTGCM originally developed at the National Center for Atmospheric Research (Bougher et al., 1990, 1999, 2000), the GFDL Mars-GCM (Wilson and Hamilton, 1996) and the model developed by the Laboratoire de Météorologie Dynamique (Paris, France), LMD-MGCM (Hourdin et al., 1993; Forget et al., 1999). With the exception of the MTGCM, all these models have been devoted to studies of the Martian atmosphere below about 80 km. Recently, in collaboration with the Instituto de Astrofísica de Andalucía (Granada, Spain), the LMD model has been extended to thermospheric altitudes, becoming the first GCM covering the whole Martian atmosphere (Angelats i Coll et al., 2005; González-Galindo et al., 2005). The MTGCM has been recently coupled to the NASA Ames MGCM, allowing also a complete coverage of the different regions of the Martian atmosphere (Bougher et al., 2004, 2006, 2009). Some other ground-to-exosphere Martian GCMs are currently under development (Takahashi et al., 2003; Moudden and McConnell, 2005; Bougher et al., 2008).

The main goal of this work is to use two General Circulation Models (GCMs), which extend from the surface up to the exobase, in order to perform an intercomparative modeling study. We are not specifically devoted here to comparisons with data, but to study the behavior of the upper Martian atmosphere from such a model intercomparison perspective.

Many different intercomparative studies between the two models are possible, as for example the comparison of the predicted neutral concentrations or the atmospheric emissions in the upper atmosphere. However, we have decided to limit this study to the comparison of the thermal and wind structure in the upper atmosphere, and their relationship with the thermal balance in the mesosphere and the thermosphere. Although the thermal balance should be the most important factor in determining the temperatures in the upper atmosphere, we are aware that maintaining such a tight focus may result in missing some scientifically interesting correlations between other variables and the temperatures/winds. Hopefully, future studies will be done that will complete the results presented here.

Both the LMD-MGCM and the MTGCM have been previously used to study some of the above mentioned observations of the Martian upper atmosphere, and in particular the thermospheric polar warming (TPW). Bougher et al. (2006) and Bell et al. (2007), using the MTGCM (coupled to the NASA Ames MGCM), found an important effect of the dust optical depth and its vertical distribution over the intensity of the TPW. González-Galindo et al. (2009b) showed the importance of the in situ heating terms in the creation of the TPW and the influence of the propagation of waves created in the lower atmosphere in its intensity. Comparisons between these published results are not easy because of the differences in the input parameters used and in the treatment of some physical processes. In this work, we have tried to minimize those differences, in particular using the same input parameters (e.g. solar flux, dust distribution, etc.), so we aim to make a coherent comparison of the thermospheric polar warming predicted by the models.

Similar comparative work has not been done before for the Martian thermosphere, and we consider it invaluable for a number of objectives. Specifically, to validate the models, to prove their ability to obtain similar results when similar inputs are used, to test the different mechanisms which couple different atmospheric layers, and to identify robust results/features of the Mars upper atmosphere which appear as non-model dependent.

In Section 2 we will present the main characteristics of both models. The scenarios chosen for this study will be described in Section 3. The results of the models and of their comparison will be analyzed in Sections 4 and 5, and in Section 6 we will summarize the main conclusions of this work.

2. The models

The Mars Thermospheric General Circulation Model, MTGCM, is a finite difference primitive equation model that self-consistently solves for time-dependent neutral temperatures, neutral-ion densities, and three component neutral winds over the globe (Bougher et al., 1999, 2000). The MTGCM is currently driven from below by the NASA Ames MGCM code at the 1.32 μbar level (60–80 km), capturing both migrating and non-migrating upward propagating tides plus the thermal expansion and contraction of the Mars lower atmosphere with the passage of the seasons and dust storm events (Bougher et al., 2004, 2006, 2009). Key prognostic (temperatures, zonal and meridional winds) and diagnostic (geopotential height) fields are passed upward from the MGCM to the MTGCM at every MTGCM grid point on 2-min timestep intervals. No downward coupling from the MTGCM to the MGCM is presently activated. The inclusion of the Ames MGCM in providing a realistic lower atmosphere is critical for achieving a realistic simulation of the Mars upper atmosphere within the MTGCM domain (Bell et al., 2007). The coupled MGCM–MTGCM framework has been used to construct inputs for the MARSGRAM 2005 empirical model (e.g. Justus and Justh, 2005; Justh and Justus, 2007) that was utilized to support Mars Reconnaissance Orbiter aerobraking.

The LMD-MGCM model evolved from a terrestrial GCM. The dynamical core solves the primitive equations by using a grid-point discretization. The adaptation to Mars was done by incorporating a package of physical processes appropriate for the Martian surface and atmosphere. It was the first Martian GCM in reproducing successfully the annual cycle of surface pressure (Hourdin et al., 1993), and it has been used in a number of studies of the Martian atmosphere (Forget et al., 1995, 1998, 1999; Montmessin et al., 2004; Angelats i Coll et al., 2004). One of the most important applications of this model is the construction of the European Mars Climate Database (EMCD) (Lewis et al., 1999) that is being currently used by many groups as a reference for atmospheric studies and also for engineering design of future missions to Mars. The LMD-MGCM has been extended to the thermosphere, becoming a ground-to-exosphere model (Angelats i Coll et al., 2005; González-Galindo et al., 2005, 2009a).

Both models include the most relevant processes for the upper Martian atmosphere. We will briefly describe here the main differences in the implementation of these processes into the models.

UV heating is the most important heating source of the Martian upper atmosphere (Houghton, 1979). LMD-MGCM considers absorption of UV solar radiation by CO_2, O_2, O, H_2, H_2O, H_2O_2 and O_3. Although only CO_2 and O have a significant effect over the UV heating in this model, it is necessary to include absorption by the other compounds to calculate their photodissociation coefficient that will then be used for photochemical calculations. In the MTGCM the constituents that absorb UV solar radiation are CO_2, O, N_2, CO and O_2. The numerical method used in the LMD-MGCM to calculate this heating term is described in González-Galindo et al. (2005). Briefly, a tabulation of the photoabsorption coefficients in 36 carefully chosen spectral intervals, based on previous work with a 1-D model, is used. For the MTGCM, regular 1-nm intervals in the range 5–240 nm are used. This is a difference with previous versions of the MTGCM (see, for example Bougher et al., 1999, 2000).

The radiative cooling rate by CO_2 emission at 15 μm, including NLTE effects, has an important role in determining the temperature structure of the upper atmosphere (e.g. Bougher et al., 1999). Both models use the same parameterization, described in López-Valverde and López-Puertas (2001), which uses a fixed atomic oxygen concentration instead of the concentration predicted by the

models (what we will call "static oxygen" scheme). The implications of this assumption are explored in Forget et al. (2009), González-Galindo et al. (2009a), and Lillis et al. (2010). In short, an overestimation of the temperatures in the upper mesosphere and the thermosphere when compared to SPICAM measured temperature profiles can be, at least in part, attributed to this assumption. The MTGCM version used in previously published papers uses a modification of this parameterization to accommodate for the atomic oxygen concentration predicted by the model (what we will call "dynamic oxygen" scheme) (Bougher et al., 2006, 2009). This modification is not used in this work.

NIR heating is included in both models using the results of López-Valverde et al. (1998). While in the LMD-MGCM an analytical fit to the tabulation presented in that work is used, the MTGCM directly uses the tabulation in the form of look-up tables. This difference should have a negligible effect over the results.

Thermal conduction is the process that provides the primary offset of UV heating (Bougher et al., 1999; González-Galindo, 2006). In both models its implementation is based on a well tested numerical solution of its governing equation. The same is true for the molecular viscosity.

Molecular diffusion determines the vertical variation of the concentrations above the turbopause (about 125 km). Both models use multicomponent diffusion, based on Dickinson and Ridley (1972, 1975), with binary diffusion coefficients. In the LMD-MGCM these coefficients are calculated following the method used in Nair et al. (1994), scaling them from the diffusion coefficient through hydrogen by using the square root of the molecular masses. For the MTGCM, bi-molecular diffusion coefficients are specified using the scheme outlined by Banks and Kockarts (1973), with individual coefficients gathered from several sources (e.g. Banks and Kockarts, 1973; Mason and Marrero, 1970; Dickinson and Ridley, 1972).

Eddy diffusion has been traditionally used in 1-D models as a means to reproduce the effects of the general circulation and of small-scale mixing over the concentration of the species (Colegrove et al., 1965). It is important in these models to include this process to obtain a well-mixed lower atmosphere. This process is also often used in GCMs to account for the small-scale mixing produced by subgrid-scale processes, such as the gravity wave breaking. In the MTGCM, a small value for the eddy diffusion coefficient is utilized (i.e. a maximum value of $10^7\,cm^2/s$ is used near the homopause). Nevertheless, the large-scale circulation does most of the vertical mixing. In the LMD-MGCM no eddy diffusion is used, as the mixing of the atmosphere is achieved by the general circulation and the parameterization of some small-scale processes, such as gravity wave drag. The implementation of this gravity wave drag in the LMD-MGCM is discussed in Collins et al. (1997) and Forget et al. (1999). It has to be noted that the gravity wave drag has been found to affect the zonal winds and the meridional circulation in the lower–middle atmosphere of Mars (Forget et al., 1999), but Angelats i Coll et al. (2005) found that the effect of this process on the upper atmosphere is quite modest. So, we do not expect important differences between the results of both models as a result of the inclusion or not of the gravity wave drag scheme.

Photochemistry is key in determining the concentrations of the different species in the upper atmosphere, and therefore, also for a correct UV heating calculation (González-Galindo et al., 2005). The LMD-MGCM solves the continuity equation for 12 species in the C, O and H families (in particular CO_2, CO, O, $O(^1D)$, O_2, O_3, H, OH, HO_2, H_2, H_2O and H_2O_2), taking into account 27 reactions between them. Photochemical equilibrium for the fastest species ($O(^1D)$, OH and HO_2) can be used to accelerate the calculations, without affecting the accuracy of the results. More information can be found in González-Galindo et al. (2005). MTGCM solves the prognostic equations for the neutral major species (CO_2, CO, N_2 and O), selected minor species (Ar, He and O_2) and several photochemically produced ions (e.g. CO_2+, O_2+, O+, CO+, NO+) (Bougher et al., 2004). No ionosphere is yet implemented in the LMD-MGCM, which can have an influence in the determination of correct neutral concentrations. In particular, the ionization of CO_2 can be a non-negligible source of atomic oxygen.

Table 1
Differences in the implementation of the physical processes in both models.

	LMD-MGCM	MTGCM
Horizontal grid (lon × lat)	5.625×4	5×5
Vertical extension	Ground to exosphere (0–250 km)	1.32 μbar – exosphere; coupled to lower atmosphere model
UV heating	CO_2, O_2, O, H_2, H_2O, H_2O_2; 36 non-regular intervals	CO_2, O, N_2, CO, O_2; 1-nm regular intervals
CO_2 15 μm	López-Valverde and López-Puertas (2001), fixed atomic O	López-Valverde and López-Puertas (2001), fixed atomic O
CO_2 NIR heating	Analytical fit to tables in López-Valverde et al. (1998)	Tabulation from López-Valverde et al. (1998)
Molecular diffusion	Multicomponent, binary coefficients	Multicomponent, binary coefficients
Eddy diffusion	No	Yes, coeff. $< 10^7\,cm^2/s$
Photochemistry	27 neutral reactions, C, O and H families	28 ion-neutral reactions

Grid size is also different on both models. While LMD-MGCM uses a 5.625×4 deg in the horizontal in the simulations shown here, with 50 levels above the surface in the vertical in σ coordinates, the MTGCM grid is 5×5 deg in the horizontal, with 33 pressure levels above 1.32 μbar. In the common range of pressures, the LMD-MGCM includes 29 layers. Both horizontal and vertical resolutions are therefore similar and should not provide important differences in the results.

Maybe the most important difference between the models is the coupling between the lower and upper atmospheres. LMD-MGCM is a ground-to-exosphere model, so it naturally couples the lower and upper atmospheres, including also the interchange with the surface. The MTGCM, as explained above, is a purely thermospheric model, so to take into account the effect of the lower atmosphere over the thermosphere it is coupled in detail (at each grid point) to a GCM of the Martian lower atmosphere (see Bougher et al., 2004, for further details).

A summary of the methods used to implement these processes in both models is presented in Table 1.

3. Common input parameters

Three basic scenarios (that is, common sets of basic input conditions) have been designed for this study. The basic idea was to keep the scenarios as simple as possible, but close to the real atmospheric conditions. The scenarios should also allow us to explore the different sources of variability in the models, paying special attention to the seasonal and dust load variability. With this is mind, we decided to use three different scenarios:

- Scenario #1: $L_s = 0$, no dust;
- Scenario #2: $L_s = 90$, shallow dust distribution (CR = 0.3);
- Scenario #3: $L_s = 270$, heavy dust load (CR = 0.03).

For the scenarios #2 and #3 the dust is homogeneously distributed in the horizontal, with a vertical structure given by a Conrath distribution (Conrath, 1975) with values 0.3 and 0.03 for the Conrath parameter, respectively.

We have tried to use as similar as possible dust opacities. However, dust opacities are defined differently (wavelength, reference pressure level, dust properties) in each of the models. Moreover the multiple scattering fast radiative models at solar wavelength used in each GCM have been shown to yield different heating rates (see Savijärvi et al., 2003, 2005). In such conditions, we have chosen to use opacity values $=0.3$ in the MTGCM and $=0.2$ in the LMD-MGCM for the scenario #2 and $=1$ and $=0.7$, respectively, for the scenario #3. These values have been used in previous comparisons between the LMD-MGCM and the NASA/AMES GCM and shown to provide good agreement for the temperatures in the lower atmosphere.

The same value for the UV and EUV heating efficiency, 18%, and for the CO_2–O deactivation rate, $3\times10^{-12}\,cm^3/s$, inside their theoretical range of variability (Fox, 1988; Shved et al., 1991; Lopez-Puertas et al., 1992; Pollock et al., 1993) have been used in both models. Also similar spectroscopic data and the same UV solar flux datasets, taken from the SOLAR2000 database (Tobiska et al., 2000) have been used for solar moderate conditions.

The models were run, starting from initial states that are different for each model but appropriate for each season, for 10 days for initialization (which allows to minimize the effects of using different initial states) and then for other 10 days in which the outputs of the models are averaged to obtain the results. All the results studied are obtained at UT$=12$.

We present in the following sections figures that illustrate the same fields as predicted by both models.

Most of the maps below are either pressure-latitude maps of zonal mean magnitudes or longitude–latitude slices at given pressure layers. Although the focus of this paper is in the mesosphere–thermosphere region (that is, the layers above about 80 km), when plotting the zonal mean temperature the vertical

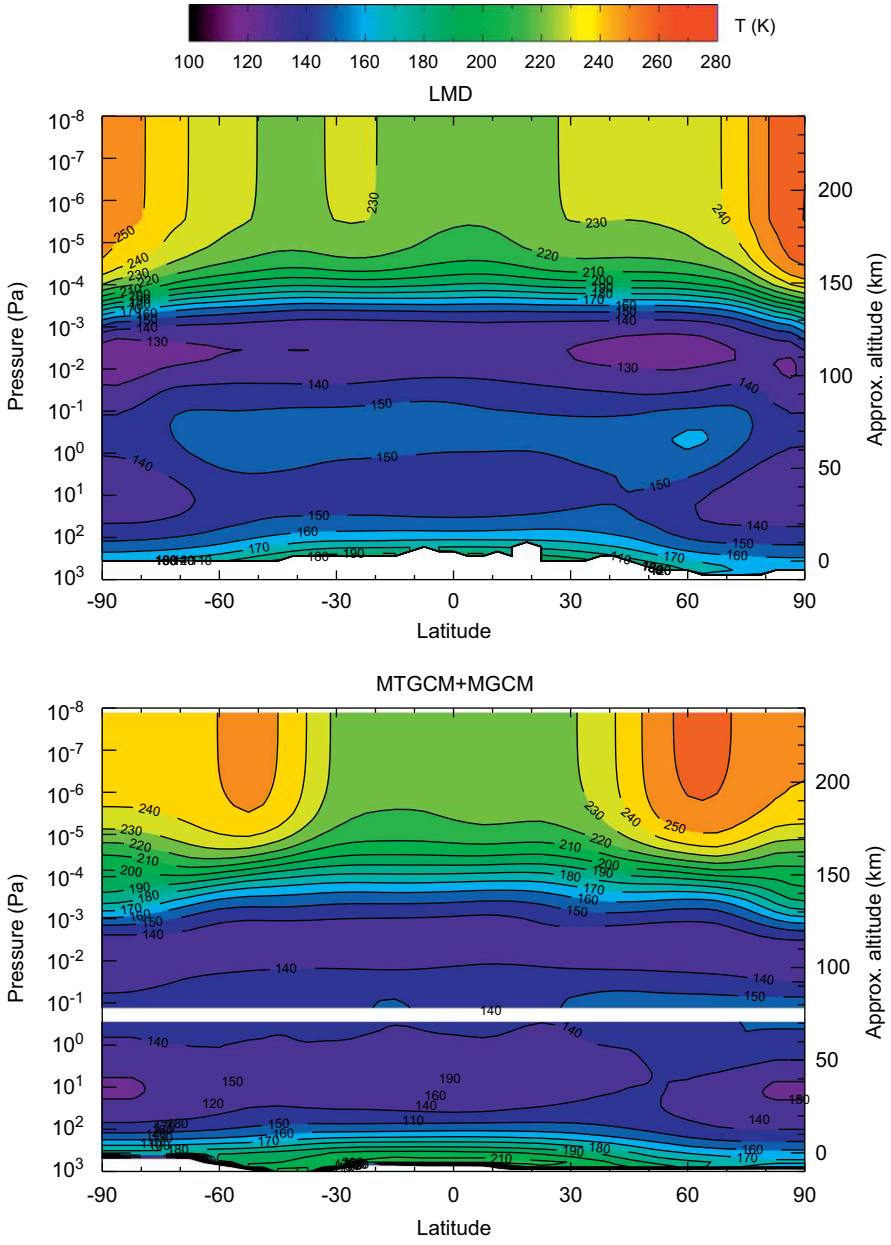

Fig. 1. Zonal mean temperatures (K) for $L_s=0$, given by LMD-MGCM (top) and MTGCM and AMES MGCM, in their regions of validity (bottom).

range chosen for representation is between the surface and 10^{-8} Pa (approximately 250 km, although this equivalence changes with season), allowing us to extend the comparison of the simulated temperatures to the lower atmosphere. That is, these plots include the lower atmosphere, the mesosphere, the mesopause region and the thermosphere, including the exobase region (that, following Valeille et al., 2010b, we can place at about 160–220 km). For this purpose, we have combined the temperatures given by the MTGCM in the upper atmosphere and those produced by the AMES-MGCM in the lower atmosphere. When plotting zonal mean values of other magnitudes, we have preferred to focus only in the upper atmosphere, and the chosen vertical range is between 0.1 and 1×10^{-7} Pa (that is, between approximately 70 and 230 km). We would like to remind the reader that the altitude values that are given together with the pressure values are only approximative, and should be considered as a rough estimation rather than as an absolute value.

4. Results for equinox

4.1. Zonal mean structure of the temperatures

Zonal mean thermospheric temperatures predicted by both models, from the surface up to the upper thermosphere (10^{-8} Pa or about 240 km) can be seen in Fig. 1. As mentioned in Section 3, for this purpose we have merged in a same plot the temperatures predicted by the MTGCM for pressures lower than about 0.2 Pa

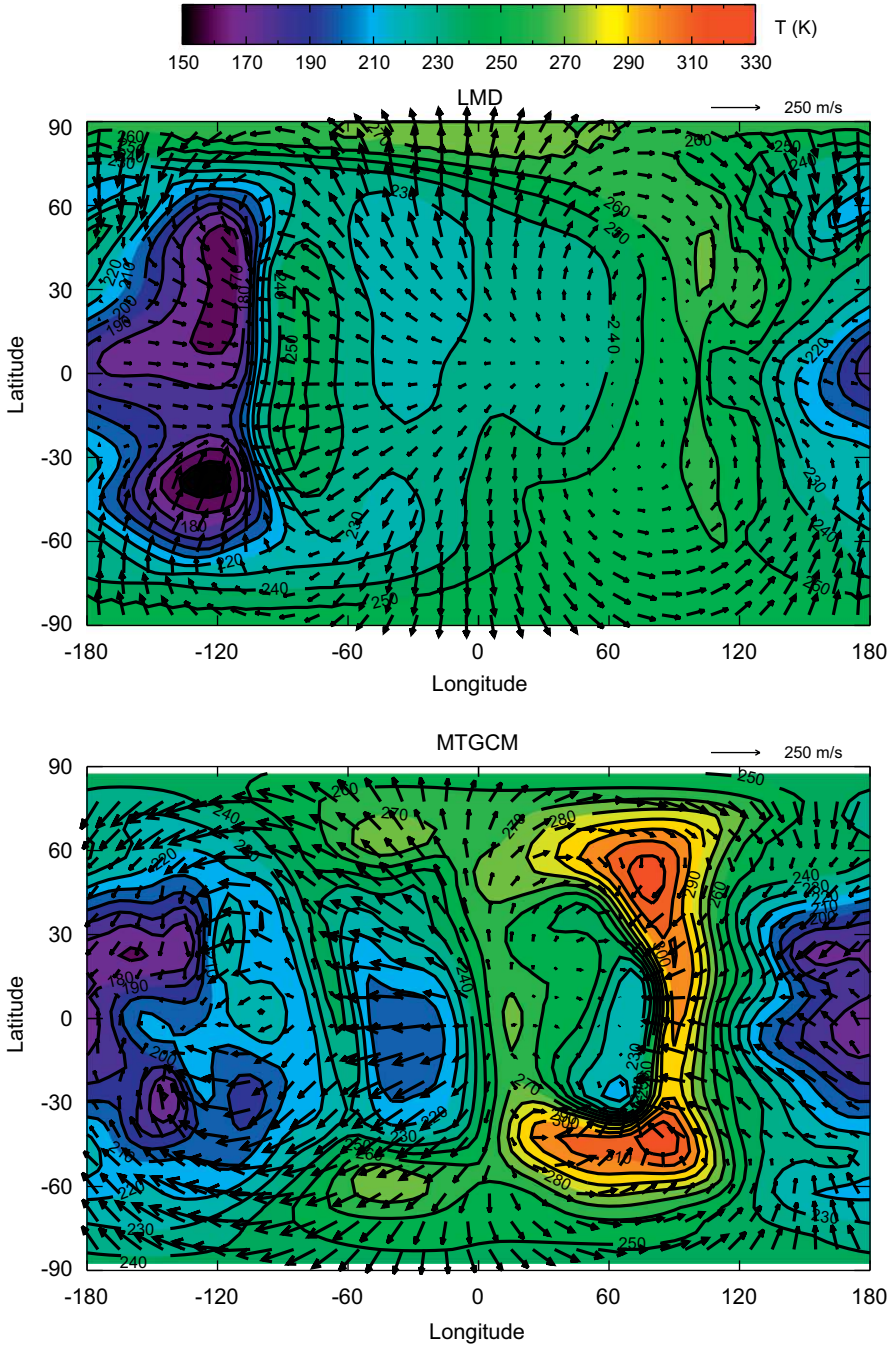

Fig. 2. Thermal (K, contour plot) and zonal and meridional wind (arrows) structure at the upper thermosphere ($P \approx 10^{-8}$ Pa, about 240 km), $L_s = 0$, given by LMD-MGCM (upper panel) and MTGCM (lower panel) for UT = 12. Longitude axis is equivalent to a local time axis (LT = 12 for lon = 0).

(that is, altitudes higher than approximately 70 km) and those predicted by the NASA Ames MGCM for pressures higher than about 0.2 Pa. The transition region between both models is marked as a white band in the plot. Both the LMD-MGCM and the MTGCM–MGCM models predict a similar vertical thermal structure. The temperatures decrease in the lower atmosphere when going from the surface to higher altitudes. Both models predict a similar double minimum structure in the lower–middle atmosphere, with minimum temperatures of about 145 K for the LMD-MGCM and $\approx$ 135 K for the NASA Ames MGCM around 10 Pa (approx. 40 km), and in the mesopause. Although below the 0.1 Pa level (about 85 km) temperatures tend to be somewhat higher in the LMD-MGCM, in the thermosphere the agreement between the models is quite good, with very similar temperatures all around the thermosphere.

Both models predict a mesopause placed at about the same pressure level (about 3×10^{-3} Pa or approximately 110 km) and with the same temperature ($\approx$ 130–135 K, with slightly lower values in the high latitudes regions). The global mean temperature of the mesopause is determined by the efficiency of IR radiative processes (Bougher et al., 1994; States and Gardner, 2000; Strobel, 2002), although some terrestrial studies show that other processes, like chemical heating and wave propagation can produce departures from this average mesopause (States and Gardner, 2000). So, the similar temperature and altitude of the mesopause in both models is indicative of a similar thermal balance at these altitudes.

Previous independent comparisons of the nighttime temperatures predicted by each model with temperature profiles measured by SPICAM in the upper mesosphere and lower

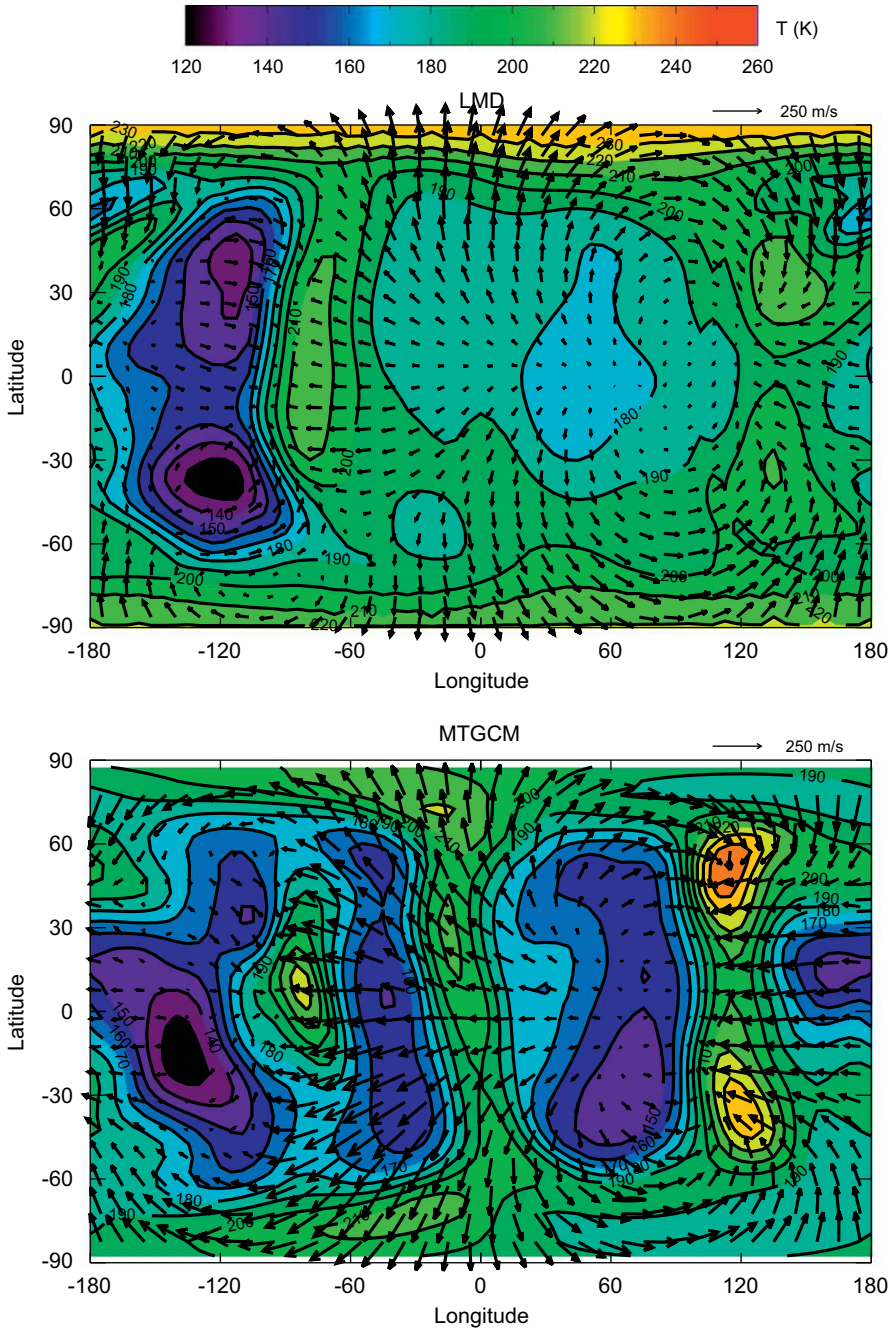

Fig. 3. Thermal (K, contour plot) and zonal and meridional winds (arrows of increasing length with intensity) structure at the lower thermosphere ($P \approx 10^{-4}$ Pa, about 150 km), $L_s = 0$, given by LMD-MGCM (upper panel) and MTGCM (lower panel) for UT = 12. Longitude axis is equivalent to a local time axis (LT = 12 for lon = 0).

thermosphere region (Forget et al., 2009) show that the models tend to overestimate the temperature of the mesopause and to underestimate its altitude (McDunn et al., 2010; Forget et al., 2009; González-Galindo et al., 2009a). It has been suggested that the differences between the LMD-MGCM results and the observations can be due to the "static oxygen" scheme (as defined in Section 2) used in the 15 μm cooling parameterization. However, the MTGCM also shows differences with the observations when using the "dynamic oxygen" scheme, which suggests that other processes, such as the dynamical heating, can be playing a role.

As stated above, other processes, distinct from radiative and dynamical ones, can have an influence on the altitude of the mesopause. Studies performed for the terrestrial atmosphere have shown that the inclusion in the models of the energy released by chemical reactions can raise the altitude of the modeled mesopause by about 10 km (Berger and von Zahn, 1999). In the Earth model, the three-body recombination of atomic oxygen and the reactions with ozone are the most important contributions to the chemical heating, which is about 10 K/day at the mesopause altitude. The MTGCM includes the chemical heating due only to the three-body recombination of atomic oxygen, while LMD-MGCM does not include any chemical heating. This might explain the low altitude of the mesopause in the models when compared to the observations. However, previous estimations done with the LMD-MGCM (González-Galindo, 2006) and MTGCM show that this heating term should be only a minor contribution to the heating balance at these altitudes.

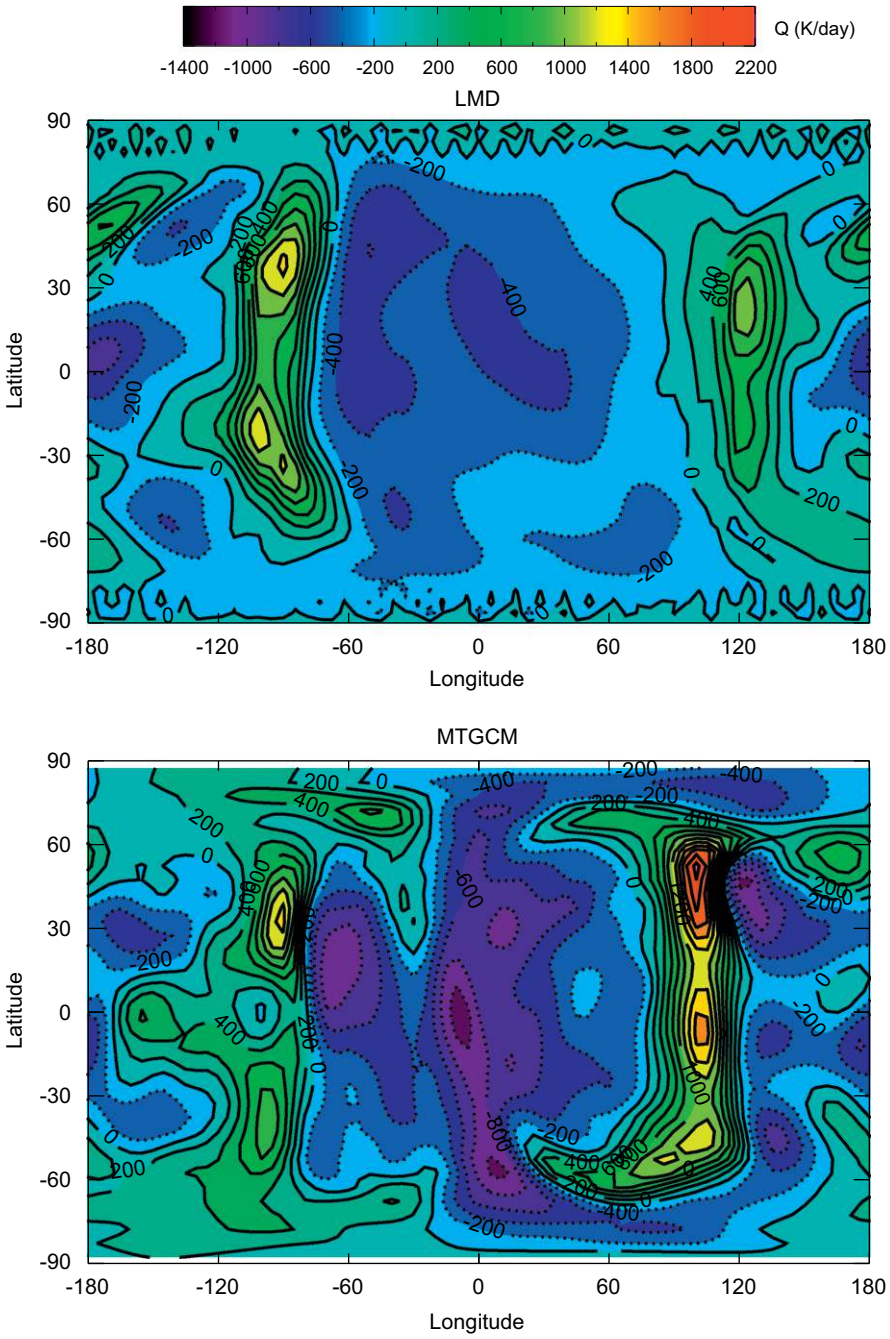

Fig. 4. Dynamic heating (K/day) structure at $P \approx 10^{-4}$ Pa (about 150 km), $L_s = 0$, given by LMD-MGCM (top panel) and MTGCM (lower panel) for UT = 12. Longitude axis is equivalent to a local time axis (LT = 12 for lon = 0).

In the upper thermosphere (layers with pressure lower than about 10^{-5} Pa, above approximately 180 km) both models predict higher zonal mean temperatures in the polar regions (around 260 K in both models, although the maximum temperatures tend to be located close to the poles in the LMD-MGCM and at about ± 60 deg latitude for the MTGCM) than in mid- and low-latitudes (220 K). This is due partially to an efficient dynamic cooling of the mid- and low-latitudes in the dayside and to the permanent illumination in polar regions at these altitudes during the equinox season. In addition, downward compressional heating owing to the equator-to-pole circulation also contributes to warm equinox temperatures near both poles (Valeille et al., 2009, 2010a).

4.2. *Longitude–latitude cross sections*

Although zonal mean maps allow us to study the big picture of the thermal and wind structure, the zonal averaging can mask some important features. Selected maps showing the variation of a given field magnitude with longitude and latitude at a fixed pressure level will allow further insight into the 3-D structure and physical behaviour of the upper atmosphere. A map illustrating the longitude and latitude variation of the temperature (color contours) and zonal and meridional winds (arrows) in a constant pressure layer in the upper thermosphere ($P=1.5\times10^{-8}$ Pa, or about 240 km, that is, well above the exobase) is shown in Fig. 2 for this equinox case. As we are showing maps for UT=12, the longitude axis can be considered as the local time axis, with midday at lon=0 and midnight at lon= $\pm$ 180, which implies that both the spatial and temporal variability are mixed.

The thermal structure predicted by both models is similar: maximum temperatures in the polar regions and in the terminator, especially in the evening, and minimum temperatures (about 170 K) close to the equator after midnight. In general, the temperatures predicted by the models are of a similar magnitude. However, there are some differences, expected when comparing these complex models. For example, the maximum temperatures in the evening terminator are higher in the MTGCM (up to 310 K) than in the LMD-MGCM (about 270 K), and the secondary maximum of temperatures close to noon (lon=0) in the MTGCM (about 270 K), that is not predicted, at least with similar intensity, by the LMD-MGCM. However, the good general agreement is not strongly affected by these differences at particular locations.

Which process or processes are responsible for this longitude–latitude structure of the temperatures in the upper thermosphere? First of all, recall that the temperatures do not change with

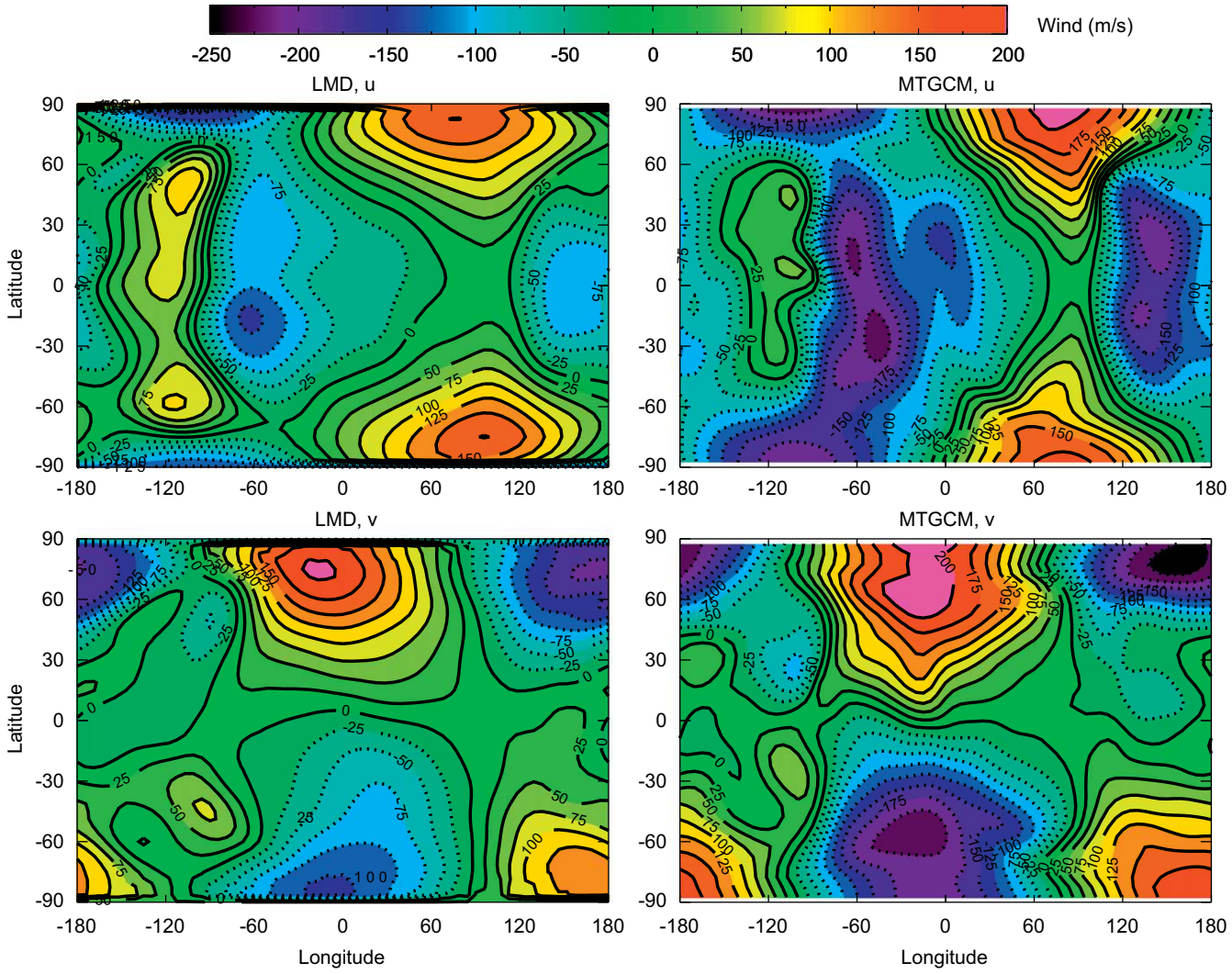

Fig. 5. Zonal (upper panels) and meridional (lower panels) winds (m/s) at the lower thermosphere ($P\approx10^{-4}$ Pa, about 150 km) given by the LMD-MGCM (left panels) and the MTGCM (right panels) for $L_s=0$ and UT=12. Longitude axis is equivalent to a local time axis (LT=12 for lon=0). Note that the contours in this plot correspond to the arrows in Fig. 3.

altitude in the upper thermosphere (above approximately 10^{-5} Pa, $\approx$180 km). Furthermore, the longitude–latitude structure of the temperatures is very similar at all levels of the thermosphere, as can be seen by comparing the temperatures in the upper thermosphere ($P=1.5\times10^{-8}$ Pa, about 240 km, Fig. 2) with the temperature structure of the lower thermosphere ($P=1\times10^{-4}$ Pa or about 150 km, Fig. 3). This implies that the temperatures at a given layer in the upper thermosphere do not only reflect local heating/cooling, but also the integrated effect over the entire thermosphere.

An examination of different layers of the longitude–latitude structure of the radiative (UV heating, NIR heating and 15 μm cooling) terms and of thermal conduction (figures not shown) shows that the UV heating and the NIR heating vary slowly over all the illuminated area, and so they cannot produce variations of temperature with longitude and latitude. The longitude–latitude distribution of the 15 μm cooling has a clear relationship with the temperature structure: the areas with higher temperature show a higher 15 μm cooling rate. This is due to the strong, non-linear dependence of this cooling term with temperature (e.g. López-Valverde et al., 1998). This means that the lon–lat distribution of the 15 μm cooling is a consequence, and not the origin, of the temperature distribution. The same can be said for the thermal conduction. So, other non-radiative process must regulate the temperature distribution.

A look at the heating effect of the winds (horizontal advection and adiabatic compression), shown in Fig. 4, reveals a clear correspondence between the areas of high (low) temperature in

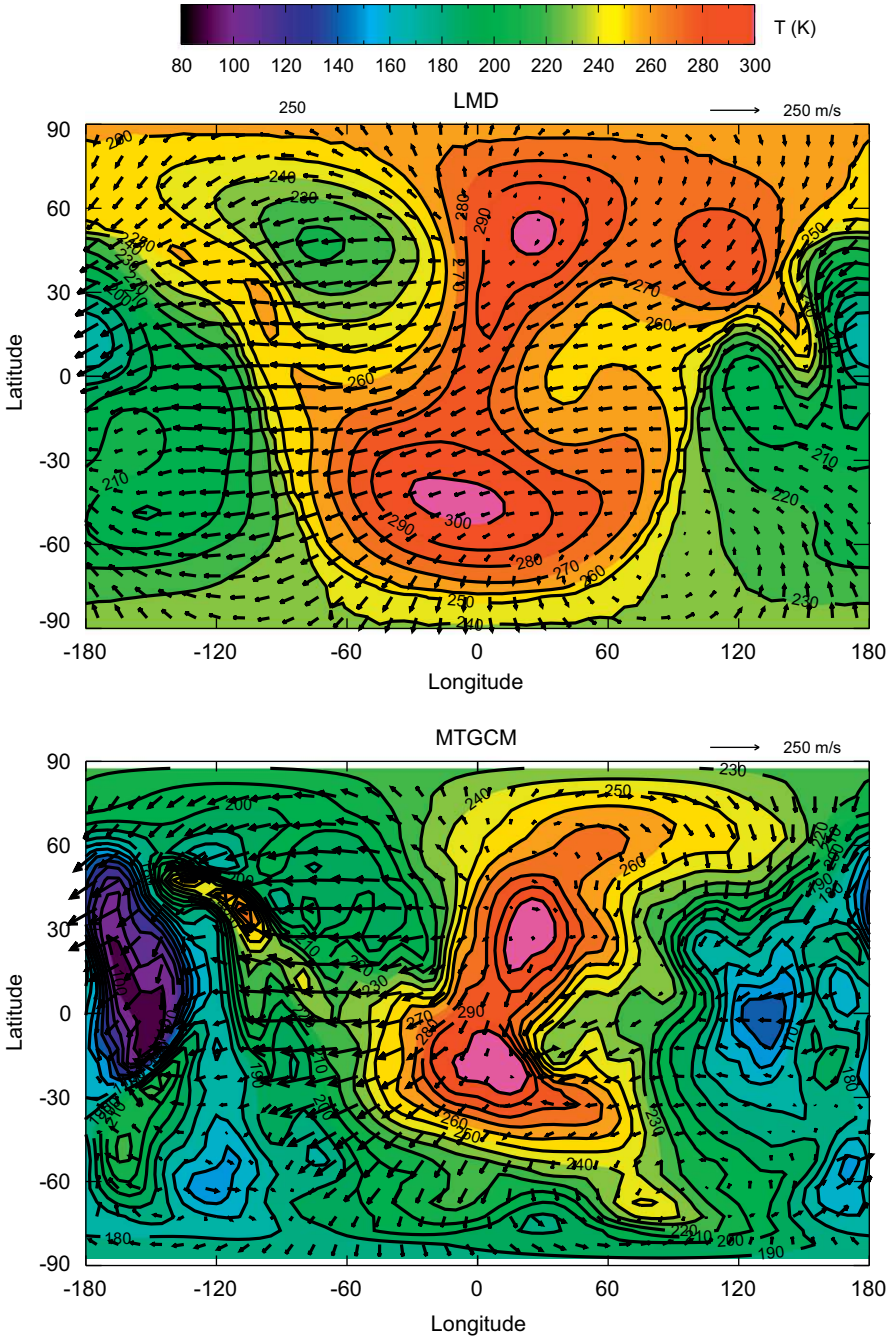

Fig. 6. Thermal (K; contours) and wind (arrows) structure at $P\approx10^{-8}$ Pa (about 220 km), $L_s=90$, given by LMD-MGCM (upper panels) and MTGCM (lower panels) for UT=12. Longitude axis is equivalent to a local time axis (LT=12 for lon=0).

the upper thermosphere ($P \approx 1 \times 10^{-8}$ Pa, or about 240 km) and the regions with high dynamic heating (cooling) in the lower thermosphere ($P \approx 1 \times 10^{-4}$ Pa, or about 150 km). This confirms the strong feedback of the dynamics on the thermal structure described by Bougher et al. (2000, 2009). Also some of the differences between the temperatures predicted by both models can be explained by Fig. 4: the higher temperatures predicted by the MTGCM at the evening terminator are related to a stronger dynamical heating predicted by this model at that particular location.

The zonal and meridional winds in the lower thermosphere ($P \approx 1 \times 10^{-4}$ Pa, or about 150 km) are shown in Fig. 5. It can be seen that both models predict a very similar wind structure, both for the zonal and the meridional components. However, MTGCM tends to predict slightly more intense winds than the LMD-MGCM. So, maximum eastward zonal winds are obtained for both models close to the pole around lon=90, but the maximum intensity is of about 210 m/s for the MTGCM and 175 m/s for LMD-MGCM. The same is true for the meridional winds, with maximum intensity around 225 m/s (both northward and southward) for the MTGCM and only 200 m/s for the LMD-MGCM.

The behaviour of the meridional winds shows that the winds diverge approximately from the Equator (corresponding to the subsolar latitude for this $L_s=0$ case) in the day hemisphere and converge in the night hemisphere. There is a clear correlation between the convergence/divergence of winds and the dynamic heating/cooling shown in Fig. 4: the areas of strong dynamic heating in the terminators are produced by a strong convergence of the winds.

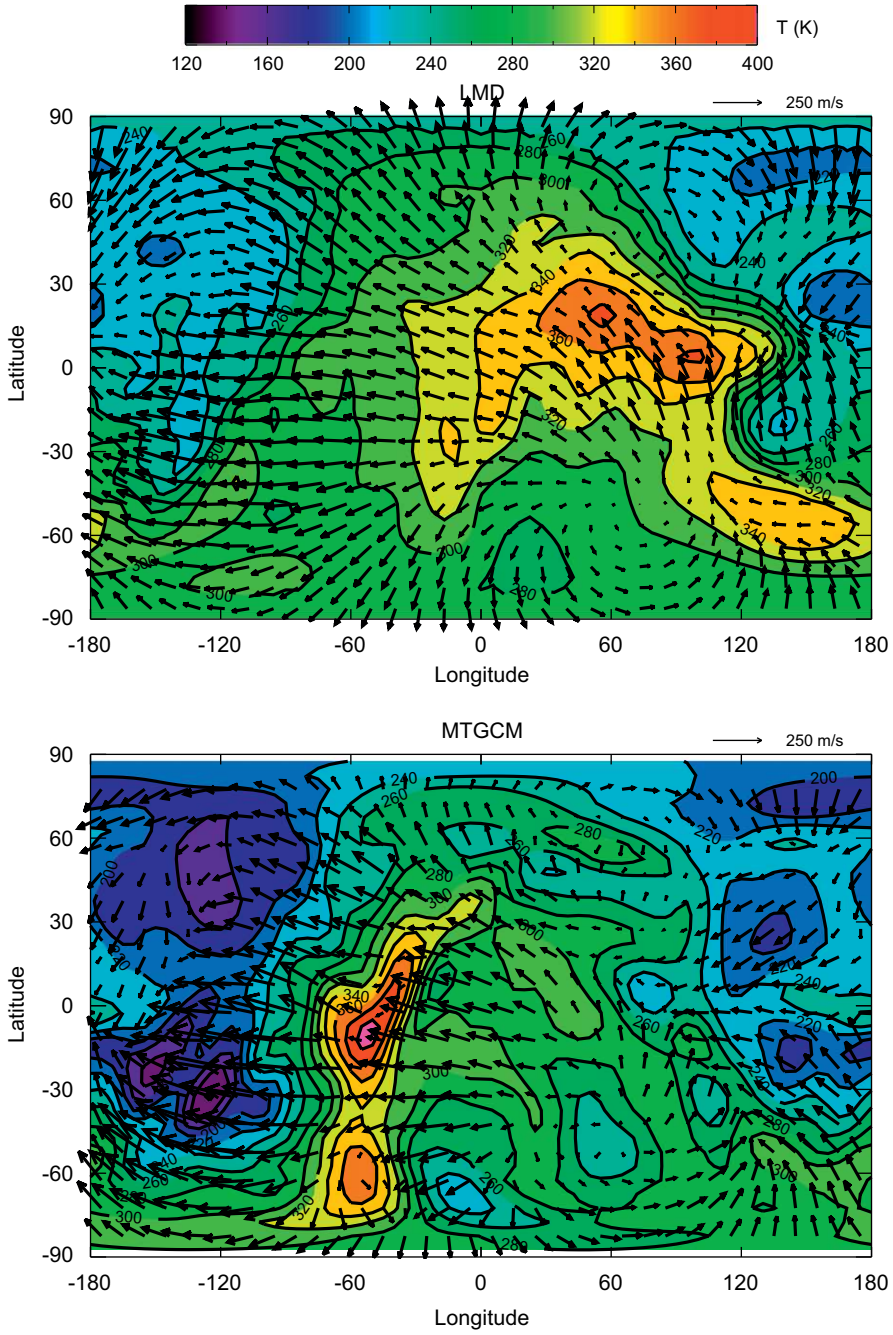

Fig. 7. Thermal (K; contours) and wind (arrows) structure at $P \approx 10^{-8}$ Pa (around 250 km), $L_s=270$, given by LMD-MGCM (upper panels) and MTGCM (lower panels) for UT=12. Longitude axis is equivalent to a local time axis (LT=12 for lon=0).

We can conclude that, even if the mean temperature in the thermosphere is determined by the balance between the different radiative heating/cooling terms and molecular conduction, the winds efficiently redistribute the energy deposited by these processes producing a longitude–latitude distribution of temperatures characterized by higher (lower) temperatures in areas with convergence (divergence) of the wind patterns.

5. Results for solstice

5.1. Longitude–latitude temperature structure

Fig. 6 shows the thermal structure in the upper thermosphere ($P \approx 1 \times 10^{-8}$ Pa, or about 220 km) for the $L_s = 90$ simulations. As for the equinox case, there is a good global agreement in the thermal structure predicted by both models, with a similar distribution of hot and cold areas. In particular, both models reflect clearly the shape of the terminator, with maximum temperatures in low latitudes in the afternoon and in mid-high Northern latitudes at the beginning of the morning, and minimum temperatures at the Equator after midnight. Both models predict an area of lower temperature in the mid-high latitudes of the Northern hemisphere after the morning terminator.

In contrast to the situation for the $L_s = 0$ case, in this case maximum temperatures are in good agreement (about 300 K in both models), but minimum temperatures are significantly higher in the LMD-MGCM (about 180 K) than in the MTGCM (about 110 K). These areas of very cold temperature in the MTGCM originate in the lower thermosphere and seem to be related to a very strong dynamical cooling, less intense in the LMD-MGCM. But in this case also the mean nighttime temperature is higher in the LMD-MGCM. This points to a difference in the heating balance between the models, but a comparison of the zonal mean heating terms does not show important differences between the models (figure not shown). Another possibility would be that the higher nighttime temperatures in the LMD-MGCM were due to a more efficient redistribution of heat from the dayside to the nightside,

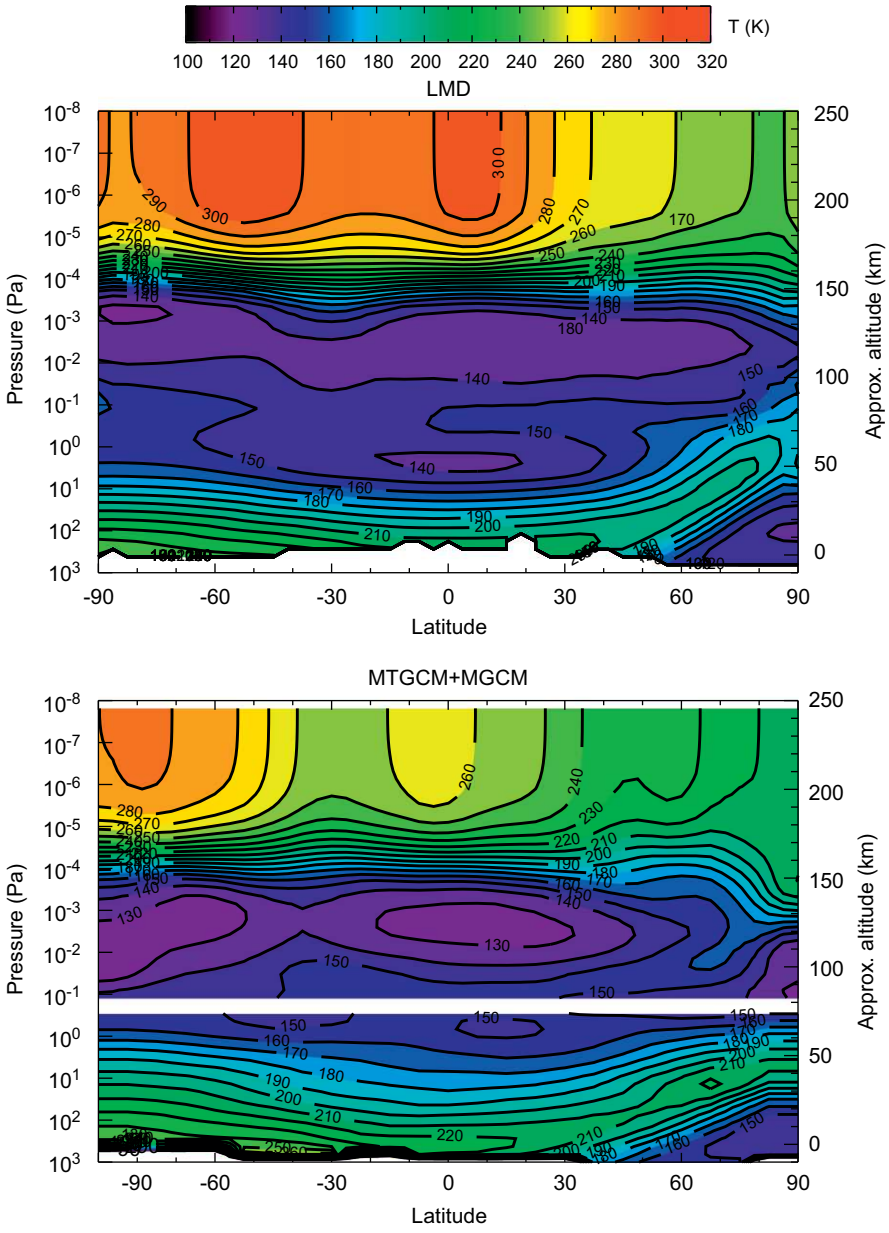

Fig. 8. Zonal mean temperatures (K) for $L_s = 270$, given by LMD-MGCM (top) and MTGCM and AMES MGCM, in their regions of validity (bottom).

but in this case the daytime temperatures should be lower in the LMD-MGCM, which is not the case.

What is the situation in the opposite season, $L_s=270$? The temperature predicted by both models at this season in the upper thermosphere ($P \approx 1 \times 10^{-8}$ Pa, or about 250 km) is shown in Fig. 7. As for the $L_s=90$ case, the shape of the terminator can be clearly distinguished in both models. In this case, MTGCM predicts higher maximum temperature (about 390, and 370 K for the LMD-MGCM) and lower minimum temperatures (around 150, 200 K for the LMD-MGCM). So, it seems that there is a general tendency for the MTGCM to predict wider day–night temperature differences. As we have seen before, these areas of extreme temperatures are related to strong dynamical heatings/coolings, so this is indicative of stronger extreme dynamical heatings/coolings in the MTGCM.

For this particular case, not only are the values of the maximum and minimum temperatures different, but also the positions of the areas of maximum temperatures are different in both models. While the MTGCM predicts maximum temperature at the beginning of the morning, the areas of maximum temperature in the LMD-MGCM are close to the evening terminator. As shown in Section 4.2, the latitude–longitude distribution of the temperature in the thermosphere is determined by the redistribution of the energy by the winds, mainly in the lower layers of the thermosphere. In this case, the MTGCM predicts a strong dynamical heating in the lower thermosphere during the first hours of the morning, while the LMD-MGCM predicts the stronger dynamical heating at the evening terminator. What produces these differences? As we will see later, the heating terms predicted by both models in the mesosphere and thermosphere region are in good agreement, so the differences in the values and position of the dynamical heating cannot be due to a dynamical response to differences in the radiative heating balance. Our hypothesis is that they are due to differences in the vertical propagation of thermal tides from the lower atmosphere. This would explain why the differences are more important for the $L_s=270$ case, when there is more dust and thus a reinforced wave activity in the lower atmosphere.

To test this hypothesis, we have studied the excitation of vertically propagating tides in the low atmosphere. An analysis of the intensity of the migrating diurnal and semidiurnal tides in the surface pressure fields produced by both models shows higher intensity for the AMES model. For the semidiurnal migrating tide, the maximum normalized amplitude is 0.023 for the AMES model and 0.015 for LMD-MGCM. For comparison, a similar study for the $L_s=0$, no dust case, shows much more similar amplitudes in both models (0.0058 for AMES model and 0.0052 for LMD-MGCM).

We want to emphasize that these differences between the models, of a local nature, are only small departures from the general situation of overall good agreement between the models. As we will see below, in spite of these local differences, the average temperatures and heating terms predicted by both models are quite similar.

5.2. Zonal mean temperature: thermospheric polar warming

The zonal mean temperatures obtained by both models for the $L_s=270$ case are shown in Fig. 8. There is a general good agreement in the thermal structure in the upper thermosphere (that is, above about 10^{-5} Pa or ≈ 180 km), with maximum zonal mean temperatures of about 300 K for the LMD-MGCM and 290 K for the MTGCM in the high latitudes of the Southern hemisphere. However, in the low–mid-latitude region, temperatures given by LMD-MGCM tend to be between about 10 and 30 K higher. Both models predict an increase of temperature when approaching the winter pole in the mesopause–lower thermosphere region (layers between 10^{-2} and 10^{-4} Pa, $\approx 110-150$ km).

As already commented in Section 1, one of the most interesting features observed in the last years in the upper Martian atmosphere is the thermospheric polar warming (TPW) detected by Mars Odyssey in the polar night for Southern summer solstice (Keating et al., 2003). The ability of the models to reproduce this feature is an interesting test of their performance. We should remind the reader that the simulations presented here are not designed to reproduce the exact conditions of MO observations. In

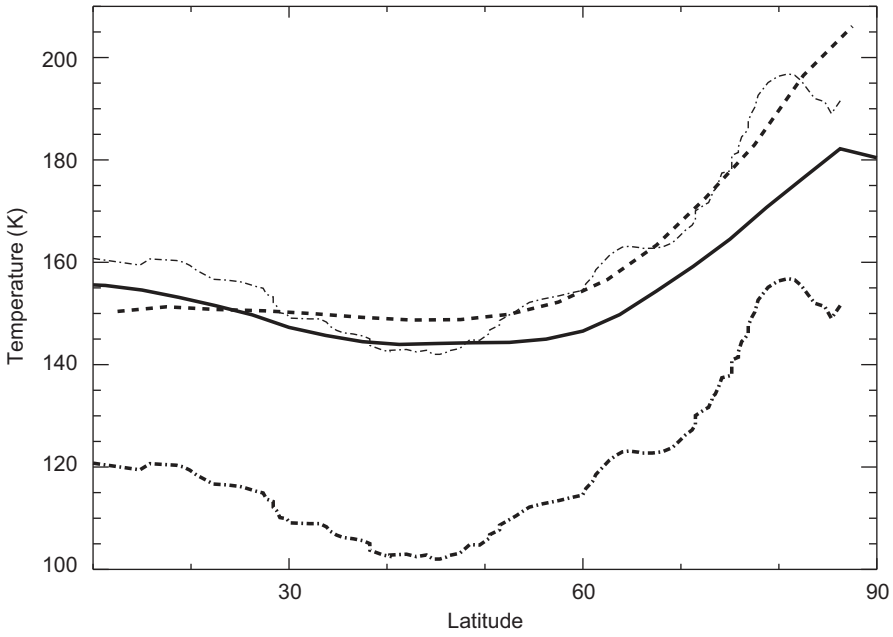

Fig. 9. Zonal mean temperature at 120 km of altitude and constant local time LT=2 for the $L_s=270$ season, given by the LMD-MGCM (solid line) and the MTGCM (dashed line). Temperature measured by Mars Odyssey for similar conditions, taken from Bougher et al. (2006) (thick dash-dotted line). Same curve, but offset by 40 K (thin dash-dotted line).

particular, as explained in Section 3, the simplified dust distribution used, although may be representative of the average conditions during the dust season, does not correspond exactly to the conditions during MO observations.

Fig. 9 shows the zonal mean temperatures predicted by the LMD-MGCM (solid line) and the MTGCM (dashed line) at 120 km and constant local time LT=2, as a function of latitude. Both models predict minimum temperature (about 145 K for the LMD-MGCM and 150 K for the MTGCM) at the same latitude, about 45 N, in good agreement with the observations by Mars Odyssey (thick dashed-dotted line). The comparison with the observations shows also that both models overestimate the temperature at this latitudinal range in between 30 and 40 K. At least part of this overestimation can be attributed to the fixed atomic oxygen concentration used in the 15 μm cooling parameterization, as described in Section 2, that is known to produce an underestimation of the cooling (e.g. Forget et al., 2009). This hypothesis is supported by previous work with the MTGCM that shows that, when using a variable atomic oxygen concentration in the 15 μm cooling parameterization, the overestimation of the nighttime temperatures is of only 10–15 K. We would like to remark that the underestimation of the 15 μm cooling should be strong in the winter hemisphere and, in particular, in the winter pole where atomic oxygen accumulates, and thus it should affect the intensity and structure of the predicted thermospheric polar warming significantly.

The intensity of the polar warming predicted by both models is different. The LMD-MGCM predicts an increase of temperature from the minimum at Lat=45 N to the pole of slightly less than 40 K, while for the MTGCM the increase of temperature is of about 58 K, similar to the $\approx$55 K warming observed by Mars Odyssey. What is producing this difference in the intensity of the thermospheric polar warming?

Bougher et al. (2006) have shown that the thermospheric polar warming is due to the dynamical heating produced by the subsidence of air in the descending branch of the Hadley cell at the polar night region during solstices. A comparison of this heating term (that combines hydrodynamical advection and

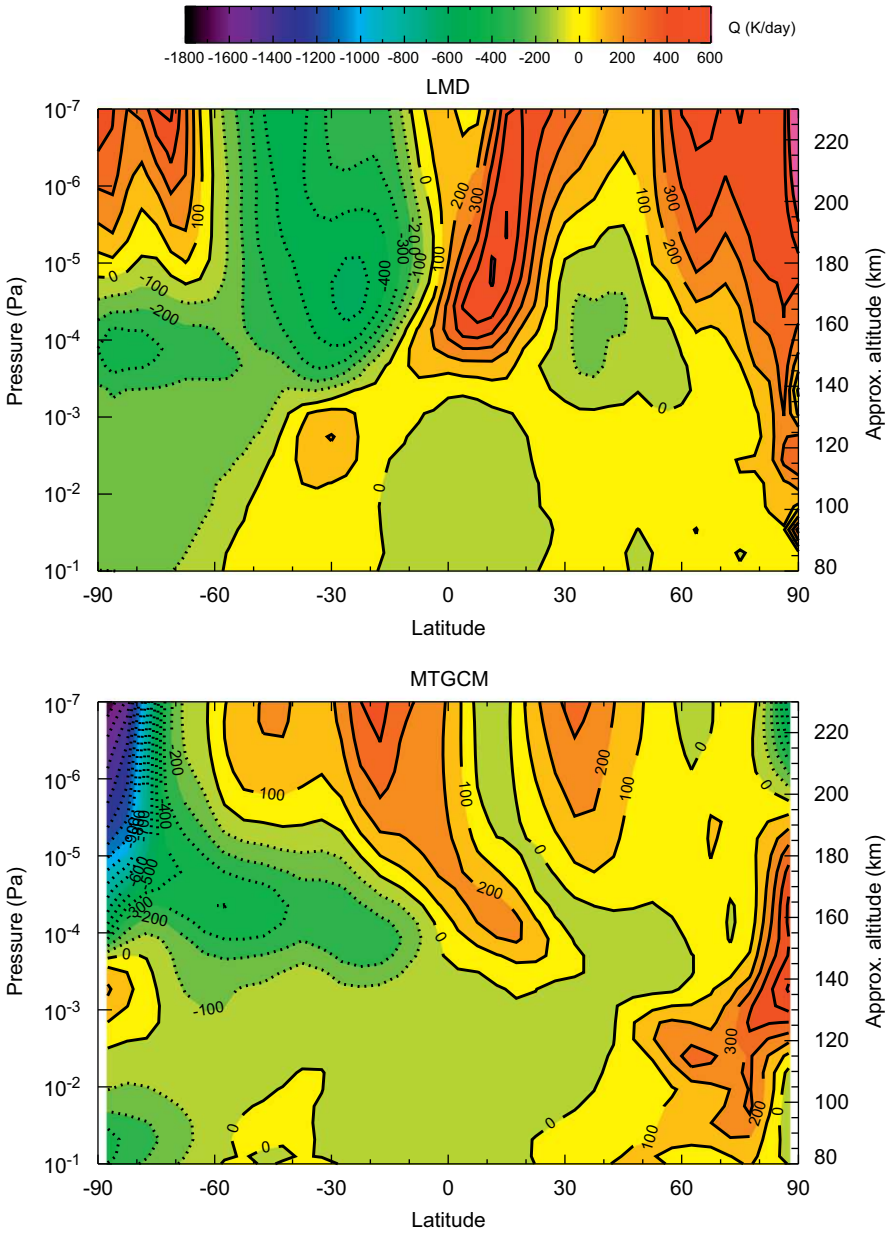

Fig. 10. Zonal mean dynamical heating (K/day) for L_s=270, given by LMD-MGCM (upper panel) and MTGCM (lower panel).

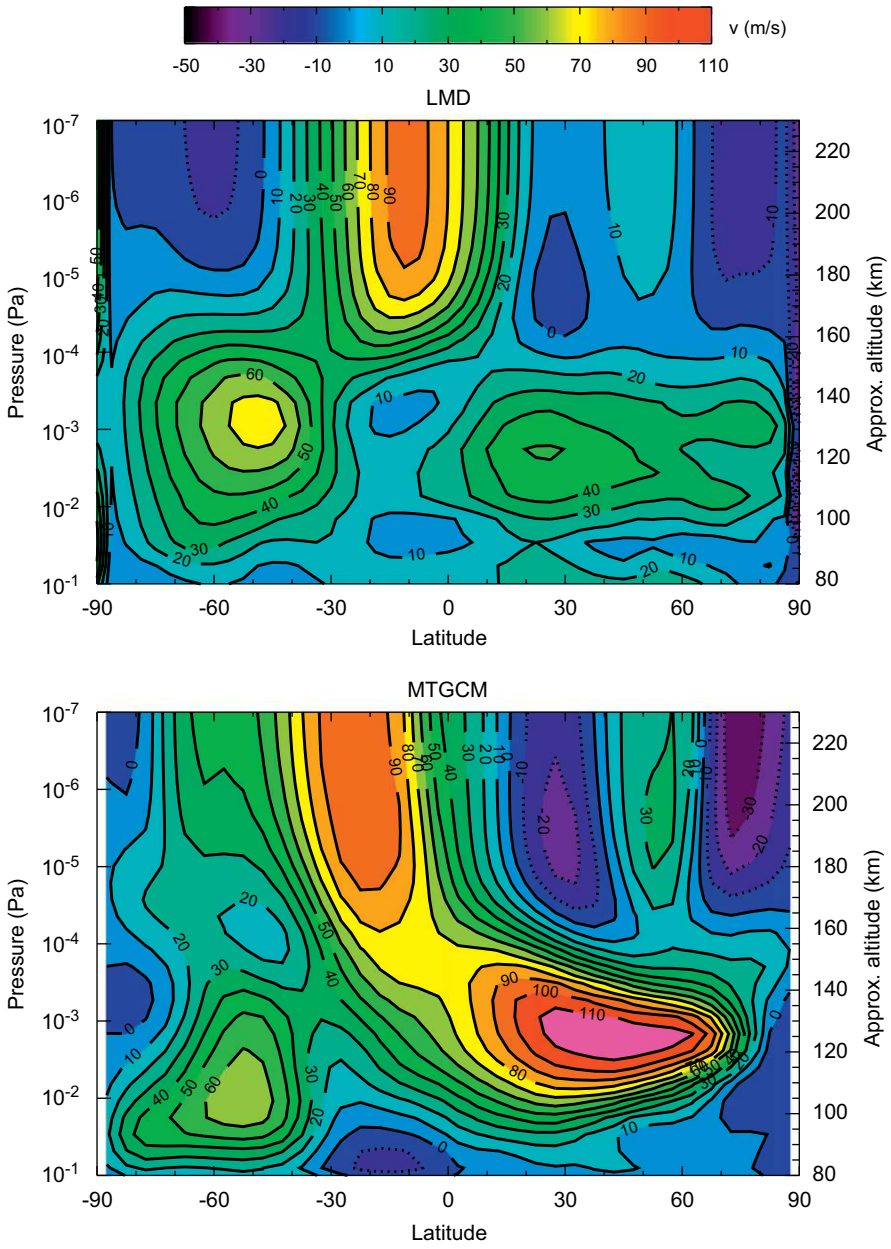

Fig. 11. Zonal mean meridional winds (m/s) for L_s=270, given by LMD-MGCM (upper panel) and MTGCM (lower panel).

adiabatical heating/cooling) as given by both models is shown in Fig. 10. Both models show a general tendency to cool the summer hemisphere and to heat the winter hemisphere, with some departures of this situation. Focusing on the polar night region, it is significant that the LMD-MGCM predicts the maximum heating in the upper thermosphere region (above 10^{-5} Pa or 180 km), where the thermal conduction is very efficient, while the MTGCM shows maximum dynamical heating in the mesopause/lower thermosphere region (between 10^{-3} and 10^{-5} Pa, around 130–180 km), where the higher density makes the thermal conduction much less efficient. In the winter polar mesopause (10^{-3} Pa, $\approx$130 km), the heating predicted by the MTGCM varies between about 200 and 500 K/day, while the LMD-MGCM predicts a more modest heating rate, between approximately 200 and 350 K/day.

This lower dynamical heating in the polar region predicted by the LMD-MGCM when compared to the MTGCM should be related to a less efficient circulation. Thus, we compare the zonal mean meridional winds obtained by both models in Fig. 11. Both models predict a change of the dynamical regime between the mesopause–lower thermosphere region, where IR balance is dominant, and the upper thermosphere, where UV heating dominates. There is a very good agreement in the meridional winds in the upper thermosphere (above about 10^{-4} Pa or 150 km), with maximum northward winds (about 95 m/s in both models) close to the Equator and weak zonal average winds in the Northern hemisphere. In the upper mesosphere/lower thermosphere region (below about 10^{-4} Pa or 150 km), although the global structure is similar in both models, with zonal mean northward winds dominating at almost all latitudes, it is clear that in the Northern (winter) hemisphere the northward winds are much more intense in the MTGCM, with a maximum wind speed of up to 110 m/s, compared to about 50 m/s in the LMD-MGCM.

Given the structure of the meridional winds at these altitudes, a zonal averaging can mask some interesting features. Longitude–latitude maps for the meridional winds at the upper

thermosphere region ($P \approx 10^{-8}$ Pa or 250 km) are shown in the upper panels of Fig. 12. In the mid- and high-latitudes of both hemisphere, the meridional winds present two jets of different sign and similar intensity (200–250 m/s). Both models present a similar wind structure, with Northward (Southward) winds during the day in the Northern (Southern) hemisphere and Southward (Northward) winds during the night in the Northern (Southern) hemisphere. The overall result is a divergence of winds from the Equator at daytime and a convergence at nighttime. Both the structure and the values of the meridional winds at this level are similar in both models, although the extreme values are higher in the MTGCM (250 m/s for 220 m/s for the LMD-MGCM).

What is the situation in the region of the mesopause (pressure around 10^{-3} Pa, $\approx$130 km), where the TPW occurs and where the zonal mean meridional wind presented differences between the models? The longitude–latitude meridional wind structure at this level is presented in the lower panels of Fig. 12. Although both models predict a similar structure, it is clear that the MTGCM predicts more intense northward winds in the low- and mid-latitudes of the Northern hemisphere (between 30 and 60 N, maximum wind is about 190 m/s for the MTGCM and 140 m/s for the LMD-MGCM). So, the differences obtained in the zonal mean meridional winds are not due to a different structure of the winds predicted by the models, but rather to a difference in the intensity of the jets at a given latitude range.

González-Galindo et al. (2009b) have shown the importance that the in situ thermal tides in the upper atmosphere have in the determination of the thermal and wind structure at these altitudes and thus on the interhemispheric circulation. These in situ thermospheric tides are created by the local heating terms, that is the CO_2 NIR heating and the UV heating. A comparison of a zonal average for these heating terms can be seen in Fig. 13. It is clear that both the NIR heating and the UV heating are globally very similar in both models. The peak heating for both terms are found at about the same levels (10^{-2} Pa, $\approx$110 km for the NIR heating and 5×10^{-6} Pa, $\approx$190 km for the UV heating), and the values of the heating are very similar (at the NIR heating peak, 190 K/day for the LMD-MGCM and 170 K/day for the MTGCM; at the UV heating peak around 1400 K/day for both models). The same can be said for the other important heating/cooling terms in the upper atmosphere, the 15 μm cooling and the thermal conduction (figures not shown).

We can thus conclude that the differences in the intensity of the meridional winds are not due to differences in the local heating/cooling terms dominant in the upper atmosphere. Most probably, these differences have their origin in the lower

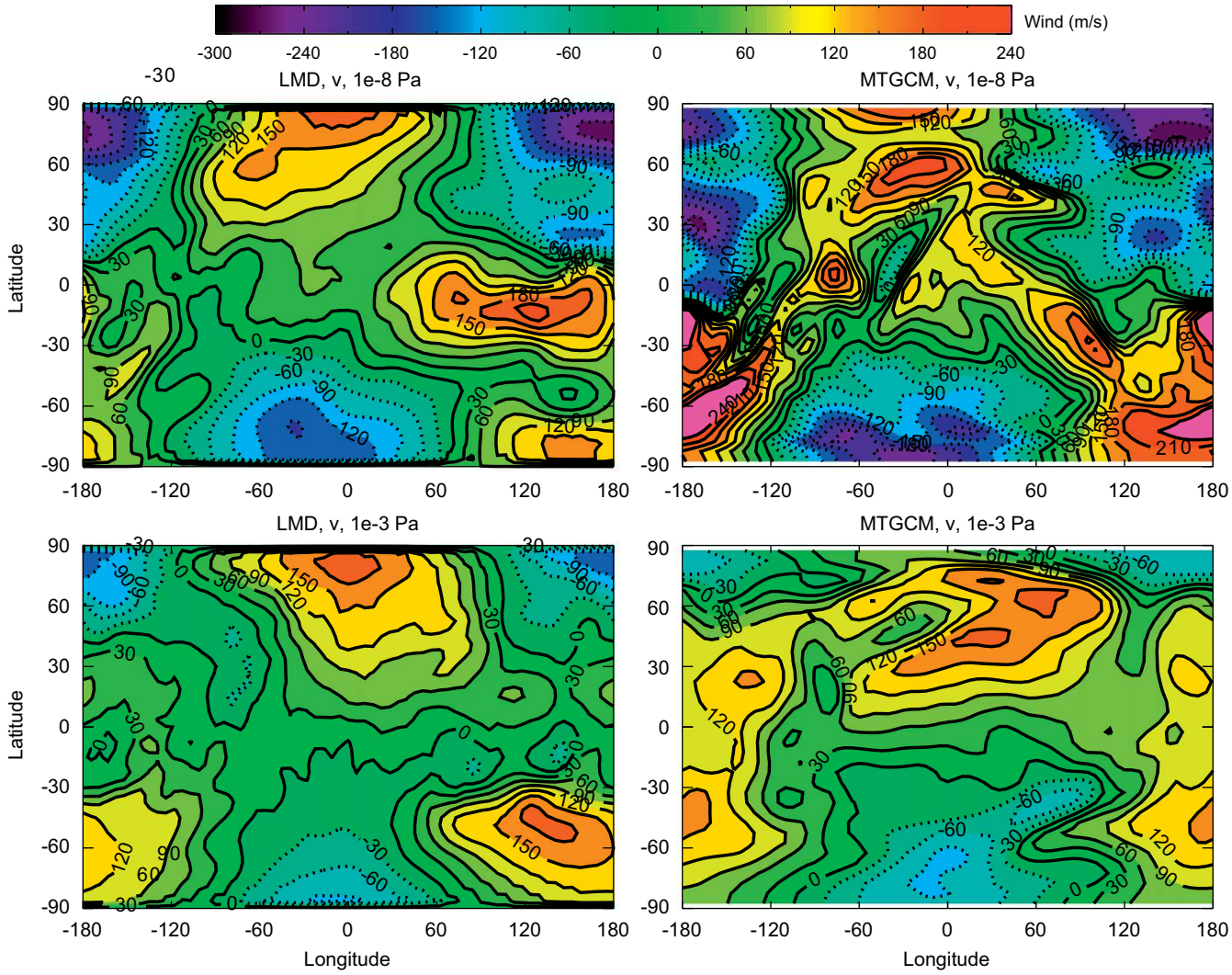

Fig. 12. Meridional winds (m/s) in the upper thermosphere ($P \approx 10^{-8}$ Pa or 250 km) (upper panels, corresponding to the meridional component of the arrows in Fig. 7) and at the mesopause level ($P \approx 10^{-3}$ Pa or 130 km) (lower panels) for L_s=270, given by LMD-MGCM (left panels) and MTGCM (right panels) for UT=12. Longitude axis is equivalent to a local time axis (LT=12 for lon=0).

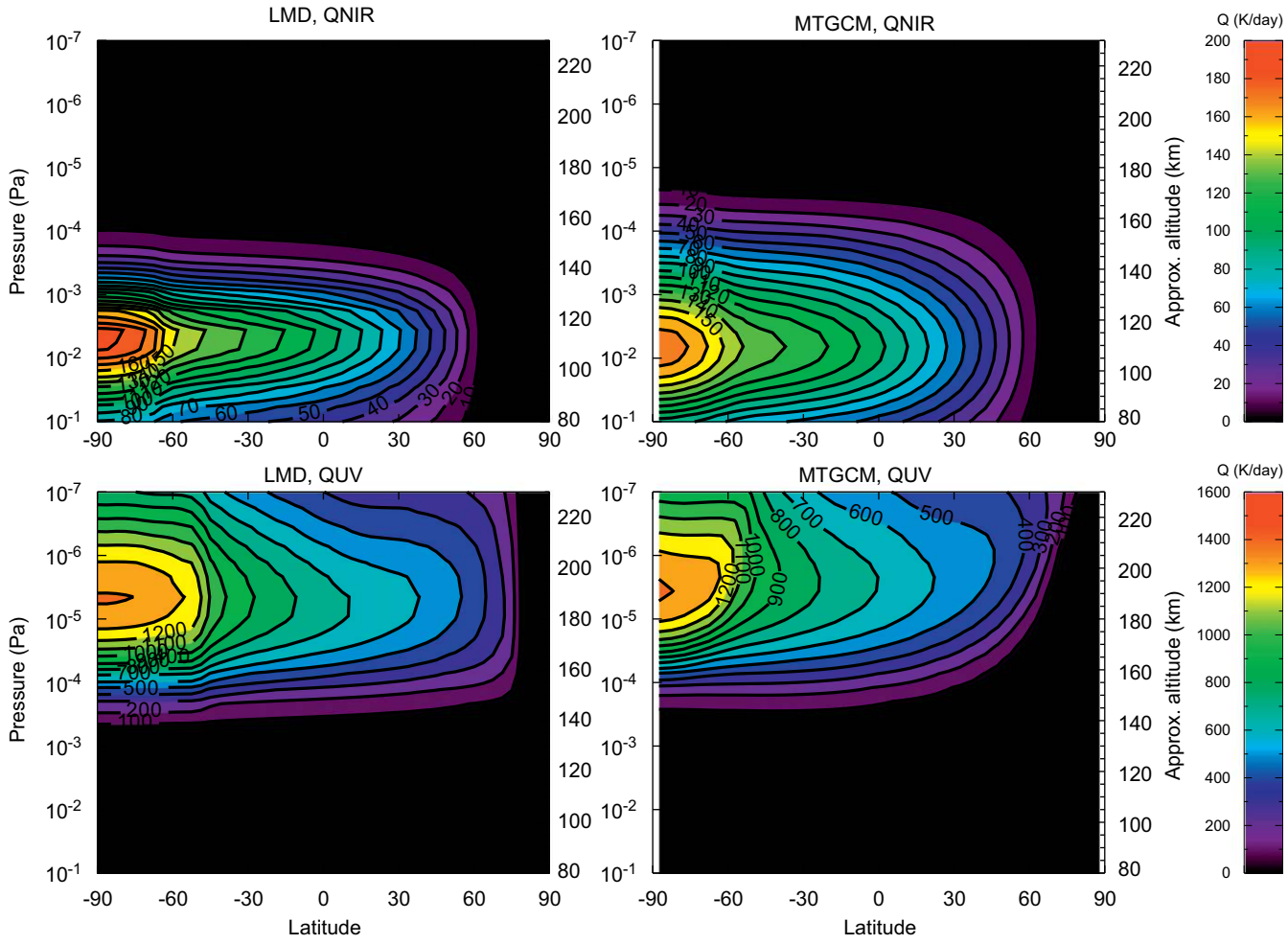

Fig. 13. Zonal mean CO_2 NIR heating (K/day, upper panels) and UV heating (K/day, lower panels) for L_s=270, given by the LMD-MGCM (left panels) and MTGCM (right panels).

atmosphere. Bougher et al. (2006) and Bell et al. (2007) have shown how the interannual variations in the dust amount in the lower atmosphere affect the thermospheric polar warming. Previous simulations with the LMD-MGCM, using similar parameters for the upper atmospheric processes (solar flux, EUV heating efficiency) but a different dust distribution in the lower atmosphere, produce a more intense polar warming, of about 60 K (González-Galindo et al., 2009b), similar to the observed one.

A look at the zonal mean temperatures in the lower atmosphere (below 0.1 Pa or about 80 km) given by both models and represented in Fig. 8 shows that the NASA Ames MGCM produces temperatures that are higher than the LMD-MGCM temperatures. In particular, around the 10 Pa level ($\approx$ 30 km above the surface) NASA Ames MGCM temperatures are between 15 and 25 K higher than LMD-MGCM temperatures, with a maximum difference of up to 40 K in the North polar region. So, the polar warming predicted by the Ames model in the lower–middle atmosphere is significantly more intense than the one predicted by the LMD-MGCM. As was mentioned, there are differences in the radiative transfer scheme used in both models that make it difficult to get the same radiative effect of suspended dust. These results suggest that these differences in the treatment of the radiative transfer in dust produce a stronger dust heating in the NASA Ames MGCM and thus a higher temperature of the lower atmosphere that, by means of a modified dynamics, produces the differences in the intensity of the thermospheric polar warming and the longitude–latitude structure of the thermospheric temperatures.

6. Conclusions

Two different global circulation models of the upper Martian atmosphere, the MTGCM and the LMD-MGCM, have been run for three different scenarios that reflect the seasonal variability of the Martian atmosphere, using similar input parameters. Our goal was to compare the global temperature and wind structures in the upper atmosphere, correlate them to the plausible heating sources as given by two different models, and identify dynamical patterns and atmospheric interactions which appear in both models.

In general, we can conclude that both models are in good overall agreement. The zonal mean structure as well as the longitude–latitude distribution of the temperatures and the winds are similar. Also the different heating terms important in the upper atmosphere are in good agreement. We have identified some differences in the models, but they are mainly of a local nature and do not affect the global agreement. These differences are more important for the scenarios with a higher dust load in the lower atmosphere. Together with the good agreement in the local heating/cooling terms in the upper atmosphere, this points to differences in the propagation of waves from the lower atmosphere as a plausible explanation to the discrepancies found between the models.

This intercomparison exercise has also allowed us to identify some features of the upper Martian atmosphere that appear in both models. We have found that the redistribution by the winds

of the energy deposited by the radiative heating terms is at the origin of the particular longitude–latitude temperature distributions found in the thermosphere. This is a further example of the importance of the dynamics in the structure of the upper atmosphere of Mars, already shown previously (Bougher et al., 2006, 2009).

Another feature reproduced by both models is the existence of the thermospheric polar warming during the perihelion season. However, this intensity is higher in the MTGCM than in the LMD-MGCM, due to a reinforced meridional transport in the upper mesosphere/lower thermosphere region. An analysis of the radiative heating terms at these altitudes shows a good overall agreement between the models. The warmer low atmosphere and a stronger excitation of migrating tides in the AMES MGCM suggests that the differences found have their origin in the lower atmosphere, and are produced by differences in the latitudinal pressure and temperature structure in the low layers of the atmosphere, and by the different propagation of tides from the lower atmosphere.

We think that this intercomparison exercise has been very useful as a way of validating the models and also to study the structure of the upper Martian atmosphere. We plan to continue the intercomparison in the future in order to study other more specific model results, like wave propagation, or temporal response to thermal and chemical perturbations at different altitudes. This exercise is open to other GCMs of the upper Martian atmosphere.

Acknowledgments

The authors wish to thank John Wilson and an anonymous referee for their useful comments. The IAA-CSIC team has been partially funded by the Spanish Ministry of Science under project AYA2008-03498/ESP and by EC FEDER funds.

References

Angelats i Coll, M., Forget, F., López-Valverde, M.A., Read, P.L., Lewis, S.R., 2004. Upper atmosphere of Mars up to 120 km: Mars Global Surveyor data analysis with the LMD general circulation model. Journal of Geophysical Research (Planets) 109, 1011.

Angelats i Coll, M., Forget, F., López-Valverde, M.A., González-Galindo, F., 2005. The first Mars thermospheric general circulation model: the Martian atmosphere from the ground to 240 km. Geophysical Research Letters 32, 4201.

Banks, P.M., Kockarts, G., 1973. Aeronomy. Academic Press, New York, London.

Bell, J.M., Bougher, S.W., Murphy, J.R., 2007. Vertical dust mixing and the interannual variations in the Mars thermosphere. Journal of Geophysical Research 112, 12002.

Berger, U., von Zahn, U., 1999. The two-level structure of the mesopause: a model study. Journal of Geophysical Research 104, 22083.

Bertaux, J.L., Leblanc, F., Perrier, S., Quemerais, E., Korablev, O., Dimarellis, E., Reberac, A., Forget, F., Simon, P.C., Stern, S.A., Sandel, B., 2005. and the SPICAM team, 2005. Nightglow in the upper atmosphere of Mars and implications for atmospheric transport. Science 307, 566–569.

Bougher, S.W., Roble, R.G., Ridley, E.C., Dickinson, R.E., 1990. The Mars thermosphere. II—general circulation with coupled dynamics and composition. Journal of Geophysical Research 95, 14811.

Bougher, S.W., Hunten, D.M., Roble, R.G., 1994. CO_2 cooling in terrestrial planet thermospheres. Journal of Geophysical Research 99, 14–609.

Bougher, S.W., Engel, S., Roble, R.G., Foster, B., 1999. Comparative terrestrial planet thermosphere 2. Solar cycle variation of global structure and winds at equinox. Journal of Geophysical Research 104, 16591.

Bougher, S.W., Engel, S., Roble, R.G., Foster, B., 2000. Comparative terrestrial planet thermospheres 3. Solar cycle variation of global structure and winds at solstices. Journal of Geophysical Research 105, 17669.

Bougher, S.W., Engel, S., Hinson, D.P., Forbes, J.M., 2001. Mars Global Surveyor Radio Science electron density profiles: neutral atmosphere implications. Geophysical Research Letters 28, 3091.

Bougher, S.W., Engel, S., Hinson, D.P., Murphy, J.R., 2004. MGS Radio Science electron density profiles: interannual variability and implications for the Martian neutral atmosphere. Journal of Geophysical Research (Planets) 109, 3010.

Bougher, S.W., Bell, J.M., Murphy, J.R., Lopez-Valverde, M.A., Withers, P.G., 2006. Polar warming in the Mars thermosphere: seasonal variations owing to changing insolation and dust distributions. Geophysical Research Letters 33, 2203.

Bougher, S.W., Blelly, P.-L., Combi, M., Fox, J.L., Muller-Wodarg, I., Ridley, A., Roble, R.G., 2008. Neutral upper atmosphere and ionosphere modeling. Space Science Reviews 139, 107–141.

Bougher, S.W., McDunn, T.M., Zoldak, K.A., Forbes, J.M., 2009. Solar cycle variability of Mars dayside exospheric temperatures: model evaluation of underlying thermal balances. Geophysical Research Letters 36, 5201.

Colegrove, F.D., Hanson, W.B., Johnson, F.S., 1965. Eddy diffusion and oxygen transport in the lower thermosphere. Journal of Geophysical Research 70, 4931–4941.

Collins, M., Lewis, S.R., Read, P.L., 1997. Gravity wave drag in a global circulation model of the Martian atmosphere: parametrisation and validation. Advances in Space Research 44, 1395–1409.

Conrath, B.J., 1975. Thermal structure of the Martian atmosphere during the dissipation of the dust storm of 1971. Icarus 24, 36–46.

Dickinson, R.E., Ridley, E.C., 1972. Numerical solution for the composition of a thermosphere in the presence of a steady subsolar-to-antisolar circulation with application to Venus. Journal of Atmospheric Sciences 29, 1557–1570.

Dickinson, R.E., Ridley, E.C., 1975. A numerical model for the dynamics and composition of the Venusian thermosphere. Journal of Atmospheric Sciences 32, 1219–1232.

Forget, F., Hansen, G.B., Pollack, J.B., 1995. Low brightness temperatures of Martian polar caps: CO_2 clouds or low surface emissivity? Journal of Geophysical Research 100 21219.

Forget, F., Hourdin, F., Talagrand, O., 1998. CO_2 Snowfall on Mars: simulation with a general circulation model. Icarus 131, 302.

Forget, F., Hourdin, F., Fournier, R., Hourdin, C., Talagrand, O., 1999. Improved general circulation models of the Martian atmosphere from the surface to above 80 km. Journal of Geophysical Research 104, 24155.

Forget, F., Montmessin, F., Bertaux, J.-L., González-Galindo, F., Lebonnois, S., Quémerais, E., Reberac, A., Dimarellis, E., López-Valverde, M.A., 2009. The density and temperatures of the upper Martian atmosphere measured by stellar occultations with Mars Express SPICAM. Journal of Geophysical Research 114, E01004.

Fox, J.L., 1988. Heating efficiencies in the thermosphere of Venus reconsidered. Planetary and Space Sciences 36, 37.

González-Galindo, F., 2006. Modelos energéticos, químicos y dinámicos de la alta atmósfera marciana. Ph.D. Thesis, University of Granada, Spain, 343pp.

González-Galindo, F., López-Valverde, M.A., Angelats i Coll, M., Forget, F., 2005. Extension of a Martian general circulation model to thermospheric altitudes: UV heating and photochemical models. Journal of Geophysical Research (Planets) 110, 9008.

González-Galindo, F., Forget, F., López-Valverde, M.A., Angelats i Coll, M., Millour, E., 2009a. A ground-to-exosphere Martian general circulation model: 1. Seasonal, diurnal, and solar cycle variation of thermospheric temperatures. Journal of Geophysical Research (Planets) 114, 4001.

González-Galindo, F., Forget, F., López-Valverde, M.A., Angelats i Coll, M., 2009b. A ground-to-exosphere Martian general circulation model: 2. Atmosphere during solstice conditions—thermospheric polar warming. Journal of Geophysical Research (Planets) 114, 8004.

Haberle, R.M., Pollack, J.B., Barnes, J.R., Zurek, R.W., Leovy, C.B., Murphy, J.R., Lee, H., Schaeffer, J., 1993. Mars atmospheric dynamics as simulated by the NASA AMES General Circulation Model. I—the zonal-mean circulation. Journal of Geophysical Research 98, 3093.

Haberle, R.M., Joshi, M., Murphy, J.R., Barnes, J.R., Schofield, J.T., Wilson, G., Lopez-Valverde, M.A., Hollingsworth, J.L., BridgerBridger, A.F.C., Schaeffer, J., 1999. General circulation model simulations of the Mars Pathfinder atmospheric structure investigation/meteorology data. Journal of Geophysical Research 104, 8957.

Houghton, J.T., 1979. Physics of Atmospheres. Cambridge University Press.

Hourdin, F., Le van, P., Forget, F., Talagrand, O., 1993. Meteorological variability and the annual surface pressure cycle on Mars. Journal of Atmospheric Sciences 50, 3625.

Justh, H.L., Justus, C.G., 2007. Mars-Gram 2005 applications for Mars Science Laboratory Mission site selection processes. In: 7th International Conference on Mars, Abstract # 3291, Pasadena, CA.

Justus, C.G., Justh, H.L., 2005. NASA Space Environment Effects Program, MARSGRAM 2005 V1.1 〈http://sec.msfc.nasa.gov/tte/model_Marsgram.htm〉.

Keating, G.M., Bougher, S.W., Zurek, R.W., Tolson, R.H., Cancro, G.J., Noll, S.N., Parker, J.S., Schellenberg, T.J., Shane, R.W., Wilkerson, B.L., Murphy, J.R., Hollingsworth, J.L., Haberle, R.M., Joshi, M., Pearl, J.C., Conrath, B.J., Smith, M.D., Clancy, R.T., Blanchard, R.C., Wilmoth, R.G., Rault, D.F., Martin, T.Z., Lyons, D.T., Esposito, P.B., Johnston, M.D., Whetzel, C.W., Justus, C.G., Babicke, J.M., 1998. The structure of the upper atmosphere of Mars: in situ accelerometer measurements from Mars Global Surveyor. Science 279, 1672.

Keating, G., Theriot, M., Tolson, R., Bougher, S., Forget, F., Forbes, J., 2003. Brief review on the results obtained with the MGS and Mars Odyssey 2001 accelerometer experiments. Paper Presented at Mars Atmosphere: Modelling and Observations Workshop, CNES-ESA, Granada, Spain, 13–15 January.

Leblanc, F., Chaufray, J.Y., Lilensten, J., Witasse, O., Bertaux, J.-L., 2006. Martian dayglow as seen by the SPICAM UV spectrograph on Mars Express. Journal of Geophysical Research 111, E09S11.

Lee, C., Lawson, W.G., Richardson, M.I., Heavens, N.G., Kleinbhl, A., Banfield, D., McCleese, D.J., Zurek, R., Kass, D., Schofield, J.T., Leovy, C.B., TaylorTaylor, F.W., Toigo, A.D., 2009. Thermal tides in the Martian middle atmosphere as seen by the Mars Climate Sounder. Journal of Geophysical Research 114, E03005.

Lewis, S.R., Collins, M., Read, P.L., Forget, F., Hourdin, F., Fournier, R., Hourdin, C., Talagrand, O., Huot, J-P., 1999. A climate database for Mars. Journal of Geophysical Research, 104.

Lillis, R.J., Bougher, S.W., González-Galindo, F., Forget, F., Smith, M.D., Chamberlin, P.C., 2010. Four Martian years of nightside upper thermospheric mass densities derived from electron reflectometry: method extension and comparison with GCM simulations. Journal of Geophysical Research 115, E07014 . doi:10.1029/2009JE003529.

Lopez-Puertas, M., Lopez-Valverde, M.A., Rinsland, C.P., Gunson, M.R., 1992. Analysis of the upper atmosphere CO_2(nu-2) vibrational temperatures retrieved from ATMOS/Spacelab 3 observations. Journal of Geophysical Research 97, 20469.

López-Valverde, M.A., Edwards, D.P., López-Puertas, M., Roldán, C., 1998. Non-local thermodynamic equilibrium in general circulation models of the Martian atmosphere: 1. Effects of the local thermal equilibrium approximation on thermal cooling and solar heating. Journal of Geophysical Research 103, 16799.

López-Valverde, M.A., López-Puertas, M., 2001. Atmospheric non-LTE effects and their parameterization for Mars. ESA Technical Report.

Magalhães, J.A., Schofield, J.T., Seiff, A., 1999. Results of the Mars Pathfinder atmospheric structure investigation. Journal of Geophysical Research 104, 8943.

Mason, E.A., Marrero, T.R., 1970. The diffusion of atoms and molecules. Advances in Atomic and Molecular Physics 6, 155–232.

McDunn, T.M., Bougher, S.W., Murphy, J.R., Smith, M.D., Forget, F., Bertaux, J.-L., Montmessin, F., 2010. Simulating the density and thermal structure of the middle atmosphere (80–130 km) of Mars using the MGCM–MTGCM: a comparison with MEx-SPICAM observations. Icarus 206, 5–17 . doi:10.1016/j.icarus.2009.06.034.

Montmessin, F., Forget, F., Rannou, P., Cabane, M., Haberle, R.M., 2004. Origin and role of water ice clouds in the Martian water cycle as inferred from a general circulation model. Journal of Geophysical Research (Planets) 109, 10004.

Moudden, Y., McConnell, J.C., 2005. A new model for multiscale modeling of the Martian atmosphere, GM3. Journal of Geophysical Research 110, E04001.

Nair, H., Allen, M., Anbar, A.D., Yung, Y.L., 1994. A photochemical model of the Martian atmosphere. Icarus 111, 124–150.

Nier, A.O., McElroy, M.B., 1977. Composition and structure of Mars' upper atmosphere—results from the neutral mass spectrometers on Viking 1 and 2. Journal of Geophysical Research 82, 4341.

Pollack, J.B., Haberle, R.M., Schaeffer, J., Lee, H., 1990. Simulations of the general circulation of the Martian atmosphere, I-Polar processes. Journal of Geophysical Research 95, 1447.

Pollock, D.S., Scott, G.B.I., Phillips, L.F., 1993. Rate constant for quenching of CO_2(010) by atomic oxygen. Geophysical Research Letters 20, 727.

Savijärvi, H., Crisp, D., Harri, A.-M., 2003. Intercomparison of lower atmosphere radiative transfer model, Paper Presented at Mars Atmosphere: Modelling and Observations Workshop, CNES-ESA, Granada, Spain, 13–15 January.

Savijärvi, H., Crisp, D., Harri, A.-M., 2005. Effects of CO_2 and dust on present-day solar radiation and climate. Mars Quarterly Journal of the Royal Meteorological Society 131, 2907–2922.

Schofield, J.T., Crisp, D., Barnes, J.R., Haberle, R.M., Magalhaães, J.A., Murphy, J.R., Seiff, A., Larsen, S., Wilson, G., 1997. The Mars Pathfinder Atmospheric Structure Investigation/Meteorology (ASI/MET) experiment. Science 278, 1752.

Seiff, A., Kirk, D.B., 1977. Structure of the atmosphere of Mars in summer at mid-latitudes. Journal of Geophysical Research 82, 4364.

Shved, G.M., Khvorostovskaia, L.E., Potekhin, I.I., Dem'ianikov, A.I., Kutepov, A.A., 1991. The measurement of the rate constant of CO_2/01 super-1 0/ quenching by atomic oxygen and the importance of the rate constant magnitude for the thermal regime and radiation of the lower thermosphere. Akademiia Nauk SSSR Fizika Atmosfery i Okeana 27, 431.

States, R.J., Gardner, C.S., 2000. Thermal structure of the mesopause region 80–105 km at 40N latitude. Part I: seasonal variations. Journal of the Atmospheric Sciences 57, 66–77.

Strobel, D.F., 2002. Aeronomic systems on planets, moons, and comets. In: Atmospheres in the Solar System: Comparative Aeronomy, Geophysical Monograph 130, AGU.

Takahashi, Y.O., Fujiwara, H., Fukunishi, H., Odaka, M., Hayashi, Y.-Y., Watanabe, S., 2003. Topographically induced north–south asymmetry of the meridional circulation in the Martian atmosphere. Journal of Geophysical Research (Planets) 108, 1–5.

Tobiska, W., Woods, T., Eparvier, F., Viereck, R., Floyd, L., Bouwer, D., Rottman, G., White, O.R., 2000. The SOLAR2000 empirical solar irradiance model and forecast tool. Journal of Atmospheric and Solar-Terrestrial Physics 62, 1233–1250.

Valeille, A., Tenishev, V., Bougher, S., Combi, M., Nagy, A., 2009. Three-dimensional study of Mars upper thermosphere/ionosphere and hot oxygen corona: 1. General description and results at equinox for solar low conditions. Journal of Geophysical Research (Planets) 114, E11005 . doi:10.1029/2009JE003388.

Valeille, A., Bougher, S.W., Tenishev, V., Combi, M., Nagy, A., 2010a. Water loss and evolution of the upper atmosphere and exosphere over Martian history. Icarus 206, 28–39 . doi:10.1016/j.icarus.2009.04.036.

Valeille, A., Combi, M., Tenishev, V., Bougher, S., Nagy, A., 2010b. A study of suprathermal oxygen atoms in Mars upper thermosphere and exosphere over the range of limiting conditions. Icarus 206, 18–27. doi:10.1016/j.icarus.2008.08.018.

Wilson, R.J., 2002. Evidence for nonmigrating thermal tides in the Mars upper atmosphere from the Mars Global Surveyor Accelerometer Experiment. Geophysical Research Letters 29.

Wilson, R.J., Hamilton, K., 1996. Comprehensive model simulation of thermal tides in the Martian atmosphere. Journal of Atmospheric Sciences 53, 1290.

Withers, P., Smith, M.D., 2006. Atmospheric entry profiles from the Mars Exploration Rovers Spirit and Opportunity. Icarus 185, 133.